BAMS Article

# The COSMIC/FORMOSAT-3 Radio Occultation Mission after 12 Years

## Accomplishments, Remaining Challenges, and Potential Impacts of COSMIC-2

Shu-peng Ho, Richard A. Anthes, Chi O. Ao, Sean Healy, Andras Horanyi, Douglas Hunt, Anthony J. Mannucci, Nicholas Pedatella, William J. Randel, Adrian Simmons, Andrea Steiner, Feiqin Xie, Xinan Yue, and Zhen Zeng

**ABSTRACT:** Launched in 2006, the Formosa Satellite Mission 3–Constellation Observing System for Meteorology, Ionosphere and Climate (FORMOSAT-3/COSMIC) was the first constellation of microsatellites carrying global positioning system (GPS) radio occultation (RO) receivers. Radio occultation is an active remote sensing technique that provides valuable information on the vertical variations of electron density in the ionosphere, and temperature, pressure, and water vapor in the stratosphere and troposphere. COSMIC has demonstrated the great value of RO data in ionosphere, climate, and meteorological research and operational weather forecasting. However, there are still challenges using RO data, particularly in the moist lower troposphere and upper stratosphere. A COSMIC follow-on constellation, COSMIC-2, was launched into equatorial orbit in 2019. With increased signal-to-noise ratio (SNR) from improved receivers and digital beam steering antennas, COSMIC-2 will produce at least 5,000 high-quality RO profiles daily in the tropics and subtropics. In this paper, we summarize 1) recent (since 2011 when the last review was published) contributions of COSMIC and other RO observations to weather, climate, and space weather science; 2) the remaining challenges in RO applications; and 3) potential contributions to research and operations of COSMIC-2.

https://doi.org/10.1175/BAMS-D-18-0290.1
Corresponding author: Shu-peng Ho, shu-peng.ho@noaa.gov
In final form 16 August 2019

**AFFILIATIONS**: **Ho**—NOAA/Center for Weather and Climate Prediction, College Park, Maryland; **Anthes, Hunt, and Zeng**—COSMIC Project Office, University Corporation for Atmospheric Research, Boulder, Colorado; **Ao and Mannucci**—Jet Propulsion Laboratory, California Institute of Technology, Pasadena, California; **Healy, Horanyi, and Simmons**—European Centre for Medium-Range Weather Forecasts, Reading, United Kingdom; **Pedatella and Randel**—National Center for Atmospheric Research, Boulder, Colorado; **Steiner**—Wegener Center for Climate and Global Change, and Institute for Geophysics, Astrophysics, and Meteorology, Institute of Physics, University of Graz, Graz, Austria; **Xie**—Texas A&M University, Corpus Christi, Texas; **Yue**—Key Laboratory of Earth and Planetary Physics, Institute of Geology and Geophysics, Chinese Academy of Sciences, Beijing, China

GPS receivers on board low-Earth-orbiting (LEO) satellites receive occulted signals from GPS satellites, which are delayed and bent due to atmospheric refraction. The observed phase delays are converted to profiles of bending angles and refractivity, which are functions of temperature, water vapor, and pressure in the troposphere, temperature and pressure in the stratosphere, and electron density in the ionosphere (Melbourne et al. 1994; Yunck et al. 2000). The Constellation Observing System for Meteorology, Ionosphere and Climate (COSMIC), consisting of six satellites in polar orbit, has successfully demonstrated the value of radio occultation (RO) data in ionosphere, climate, and meteorological research and operational numerical weather prediction (NWP).

By the middle of 2019, COSMIC has provided more than seven million RO soundings. More than 3,700 people from 86 countries have registered as users of the data and over 1,000 COSMIC-related journal papers have been published.

Although all of the six COSMIC GPS receivers were designed with a lifetime of two years from launch, many of the satellites continued to provide data well beyond 2008, providing more than 1,000 soundings per day through 2016 (Fig. 1). However, by the middle of 2019, only one of the original six satellites was still producing data. Other RO missions including *Satellite de Aplicaciones Cientificas-C (SAC-C)* and Gravity Recovery and Climate Experiment (GRACE) in a research mode and *Meteorological Operational Satellite Program (MetOp) A/B*, *GRACE-A*, *TerraSAR-X (TSX)*, *Communications/Navigation Outage Forecasting System (C/NOFS)*, *TerraSAR-X Add-On for Digital Elevation Measurement (TanDEM-X)*, *Fengyun-3C (FY-3C)*, and *Korea Multi-Purpose Satellite-5 (KOMPSAT-5)* in near–real time (NRT) have compensated for some of the loss; however, the total number of RO observations available in NRT by the end of 2018 was about 1,700, down from a maximum of over 3,500 in 2007–09.

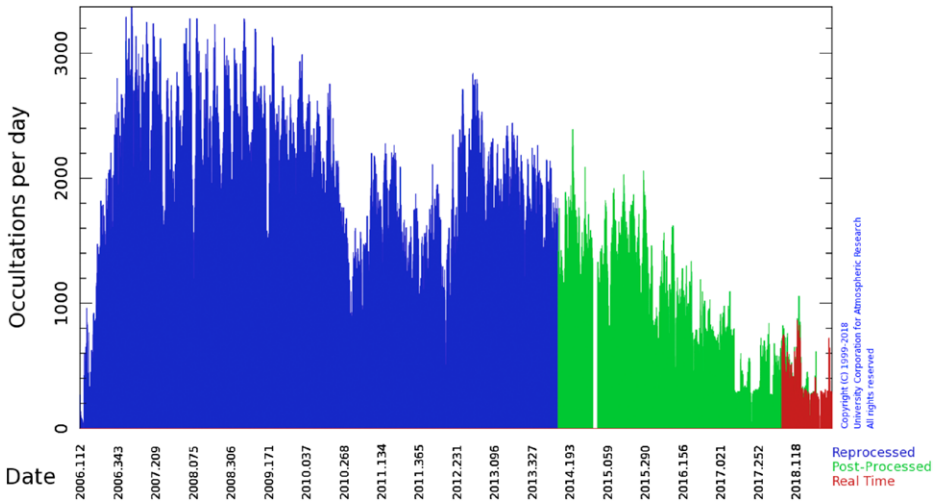


**Fig. 1. Number of RO vertical profiles from COSMIC processed by UCAR CDAAC from 21 Apr 2006 to 6 Dec 2018 (DOY 340).**

A COSMIC follow-on mission, COSMIC-2, was launched on 25 June 2019. With six LEO satellites in 24° inclination orbits, COSMIC-2 will collect at least 5,000 RO soundings per day from the GPS, Galileo, and Global Navigation Satellite System (GLONASS) satellite navigation systems over the tropics and subtropics from 35°N to 35°S, providing an average of about seven soundings

per day in each 5° × 5° latitude box (compared to about one sounding per day in each per 5° × 5° latitude box for COSMIC-1). COSMIC-2 will use an advanced receiver known as GPS, GALILEO, and GLONASS (TriG) Global Navigation Satellite System (GNSS)-RO Receiver System (TGRS) developed by the Jet Propulsion Laboratory and a digitally beam-steered antenna. Compared to the COSMIC-1 receiver, the TriG will have a significantly increased signal-to-noise ratio (SNR) of approximately 1,600 dB, 2 times that of COSMIC-1. In addition to the TGRS, secondary payloads on the COSMIC-2 satellites include two space weather instruments, an ion velocity meter and radio frequency beacon transmitter (Yue et al. 2014). COSMIC-2 satellites will also provide high-rate (50 Hz) data of the ionosphere to observe scintillation. These improvements, though limited to the tropics and subtropics, will increase the value of RO observations for weather, climate and space weather research and especially tropical cyclone forecasting.

Anthes et al. (2008) and Anthes (2011) reviewed the COSMIC science achievements from 2006 to 2011. Bonafoni et al. (2019) reviewed contributions of RO to understanding and predicting extreme events. In this paper, we provide recent examples of contributions of COSMIC and other RO missions to phenomenological studies (second section), advances in numerical weather prediction and data assimilation (third section), climate (fourth section), and space weather science (fifth section). Remaining challenges for using RO data and potential benefits of COSMIC-2 are also discussed in the sixth section.

## Observational studies of atmospheric processes

RO data provide valuable and unique atmospheric information because of their high accuracy and precision, high vertical resolution, insensitivity to clouds and precipitation, and global coverage (Kursinski et al. 1997, 2000; Collard and Healy 2003; Kuo et al. 2004; Ho et al. 2009a,b; Anthes et al. 2000; Anthes 2011; Anthes and Rieckh 2018). In this section, we highlight selected observational studies using RO and other satellite data on atmospheric waves, deep convection, and tropical cyclones.

***Atmospheric waves.*** With high vertical resolution of between 200 and 600 m (Zeng et al. 2019), RO temperature profiles can resolve different types of gravity waves (GW) in the lower stratosphere (Alexander et al. 2008a,b; Luna et al. 2013). GW studies using COSMIC data include (i) regional and global GW structures and their variability (Alexander et al. 2008a; McDonald 2012; Tsuda 2014; Khaykin et al. 2015), (ii) interaction of GW with the background flow (Nath et al. 2015), (iii) impact of GW on the tropopause (Kim and Alexander 2015) and cirrus cloud formation (Alexander et al. 2011), (iv) GW excitation mechanisms over different regions (Ming et al. 2014; Hindley et al. 2015), and (v) evaluation of GW representation in the models or other observations (Alexander et al. 2008a; Tsuda 2014). A unique aspect of the COSMIC constellation is that it provides multiple nearby observations for estimating GW parameters (Wang and Alexander 2010; Faber et al. 2013; Schmidt et al. 2016). Figure 2 shows GW horizontal and vertical wavelengths, intrinsic frequency, and momentum flux derived from three or more nearby RO temperature profiles using cross-wavelet analysis. These parameters, which are estimated with a vertical resolution and accuracy that cannot be obtained by other remote sensing techniques, are valuable in constraining GW parameterizations in NWP and climate models.

RO also contributes to our understanding of planetary-scale stratospheric waves. In a study of Arctic and Antarctica waves, Alexander and Shepherd (2010) found short-lived (less than two weeks) waves with wavelengths less than 5 km throughout the winters of both hemispheres. Enhanced planetary waves precondition the stratospheric circulation prior to Arctic sudden stratospheric warmings. In the Southern Hemisphere, planetary waves are typically quiescent in summer, though an exception occurred in December 2006–February 2007 (Shepherd and Tsuda 2008). Using RO data, Alexander et al. (2008b) and Randel and Wu (2005) studied convectively coupled equatorial waves. Brahmanandam et al. (2010), Pan et al. (2011), and Flannaghan and Fueglistaler (2013) studied the

structures of Kelvin waves and their variability with longitude, seasons, quasi-biennial oscillation (QBO), and El Niño–Southern Oscillation (ENSO). The Kelvin waves were confined to 30°W to 90°E in boreal winter, but propagated over most longitudes in boreal summer. The frequency of Kelvin waves in the stratosphere was high during the easterly phase of the QBO and maximum when the easterlies changed to westerlies. Kelvin waves dominated the subseasonal variability of the tropical tropopause, modulated the tropopause height and temperature, and varied in consonance with deep convection (Scherllin-Pirscher et al. 2017).

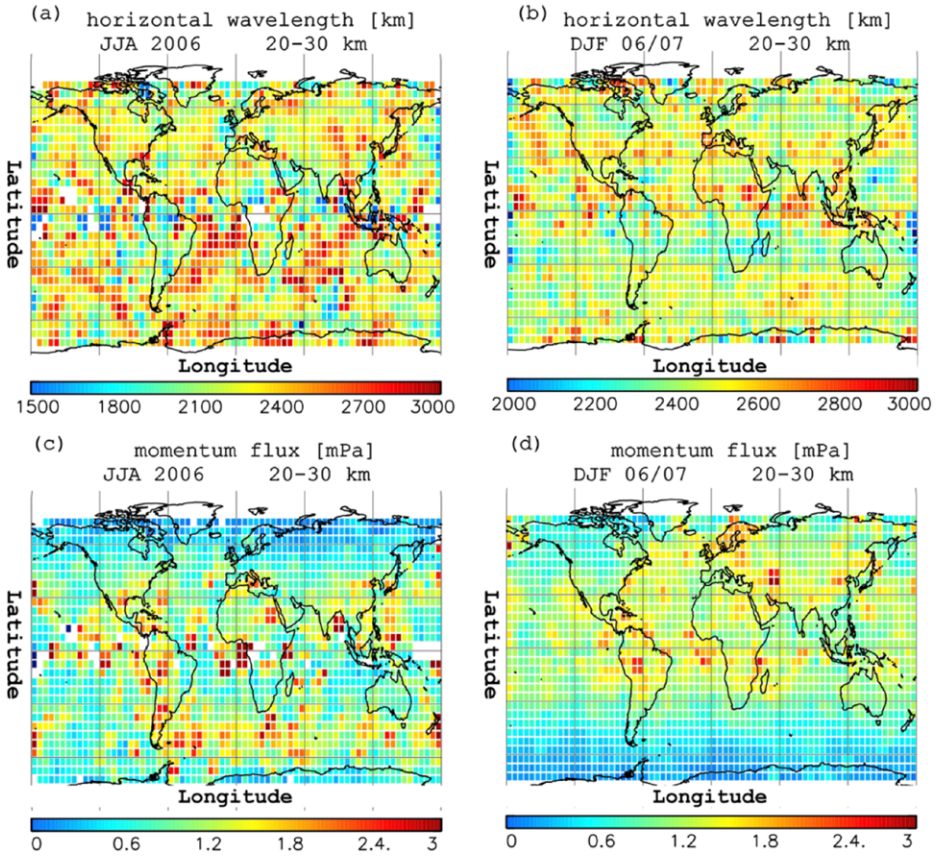


**Fig. 2. (a),(b) Horizontal wavelengths and (c),(d) momentum fluxes derived from COSMIC temperature profiles for (left) JJA 2006 and (right) DJF 2006 (Faber et al. 2013, their Fig. 10).**

Tian et al. (2012), using RO and Atmospheric Infrared Sounder (AIRS) data, documented the spatiotemporal patterns and vertical structure of the temperature variability in the upper troposphere and lower stratosphere (UTLS) associated with the Madden–Julian oscillation (MJO). Many detailed finescale vertical structures of temperature anomalies between 150 and 50 hPa were resolved by RO, but not by AIRS. In addition, the equatorial temperature anomalies at 250 hPa over the Indian and western Pacific Ocean from RO showed significantly larger magnitudes compared to those from AIRS. These differences can be explained by the lower sampling of AIRS in the presence of optically thick clouds and lower vertical resolution near the tropopause, compared to RO. GPS RO moisture anomalies associated with the MJO are generally similar to AIRS and ERA-Interim (Zeng et al. 2012). As shown in Fig. 3, all anomalies propagated from the Indian Ocean to the central Pacific with the deep convection anomaly. Significant warm temperature anomalies with peak amplitude of 0.6 K between 800 and 200 hPa were accompanied by cold anomalies tilting eastward with height near the tropopause (150–70 hPa). The vertical structure of moisture anomalies tilted westward, resulting in a low-level moistening that precedes the MJO convection. Virts and Wallace (2014) extended analyses of the MJO, establishing the connections between temperature, cirrus clouds, and trace gases in the tropical tropopause layer and their responses to planetary-scale anomalies. These studies demonstrated that this dataset will be valuable for evaluating climate model performance for equatorial temperature anomalies.

***Deep convection and tropical cyclones.*** Numerous studies have used RO measurements to evaluate the impact of deep convection on the UTLS. Biondi et al. (2012) investigated the thermal structure associated with deep convective systems. Systematic anomalies in RO bending angles closely aligned with the top of convective systems, corresponding to anomalously cold temperatures (Fig. 4). For cloud tops below 14 km, the temperature lapse rate within the cloud

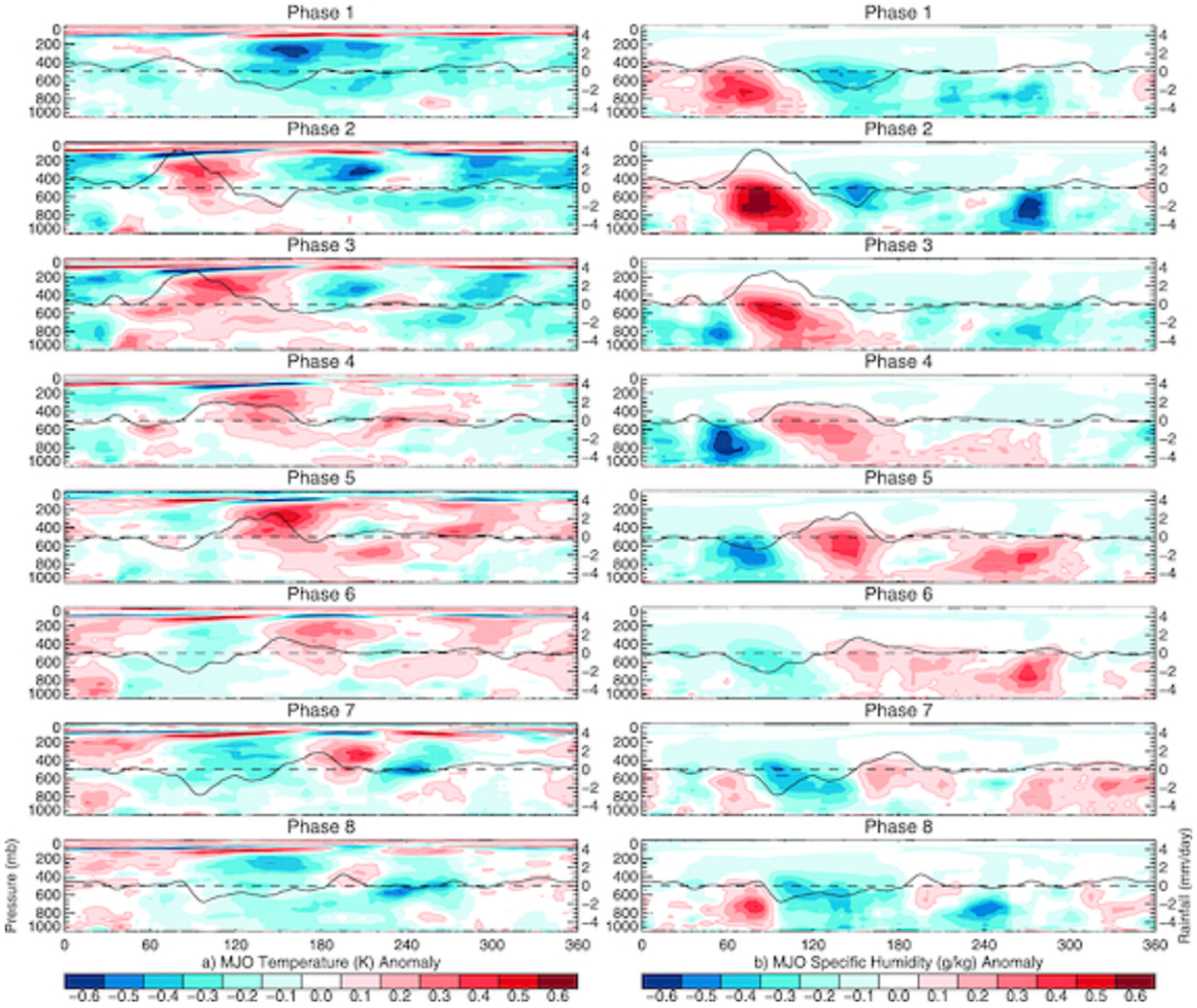


**Fig. 3. Vertical structure of (left) RO temperature and (right) specific humidity MJO anomalies (shading) averaged over 10°S–10°N for a composite cycle (8 phases). The overlaid solid black lines are Tropical Rainfall Measuring Mission (TRMM) MJO rainfall anomalies (proxy for convective intensity, scale at right) for the same period of COSMIC RO data (Zeng et al. 2012).**

often approaches a moist adiabat, consistent with rapid undiluted ascent. Above the cloud top the lapse rate typically becomes negative, corresponding to the inversion in the temperature profiles above cloud top. Kim et al. (2018) quantified cooling of the tropical tropopause linked to extreme deep convection, including effects of the cooling on stratospheric water vapor.

Biondi et al. (2011, 2013) demonstrated that RO data can detect the variation of cloud-top heights in tropical cyclones (TC). Biondi et al. (2015) computed mean vertical temperature profiles for TCs over all ocean basins. They selected more than 20,000 RO profiles collocated with TCs and classified them by intensity of the cyclone and by ocean basin. The results show that TC have different cloud-top heights and temperature characteristics depending on the basin. The temperature usually shows a negative anomaly near the cloud top. In the Northern Hemisphere, the temperature anomaly becomes positive above the cloud top, while in the Southern Hemisphere, the anomaly remains negative up to about 25 km.

Despite the long horizontal averaging scale (~200 km), Vergados et al. (2013) showed that RO observations from Challenging Minisatellite Payload (CHAMP) and COSMIC could resolve, albeit in a smoothed way, the major characteristics of TC structure—the eye and eyewall, the inflow and outflow layers, and even rainbands in a composite of 42 North Atlantic TCs over the period 2002–10 (Fig. 5). Thus many continuous and widespread RO observations in the tropics (as in

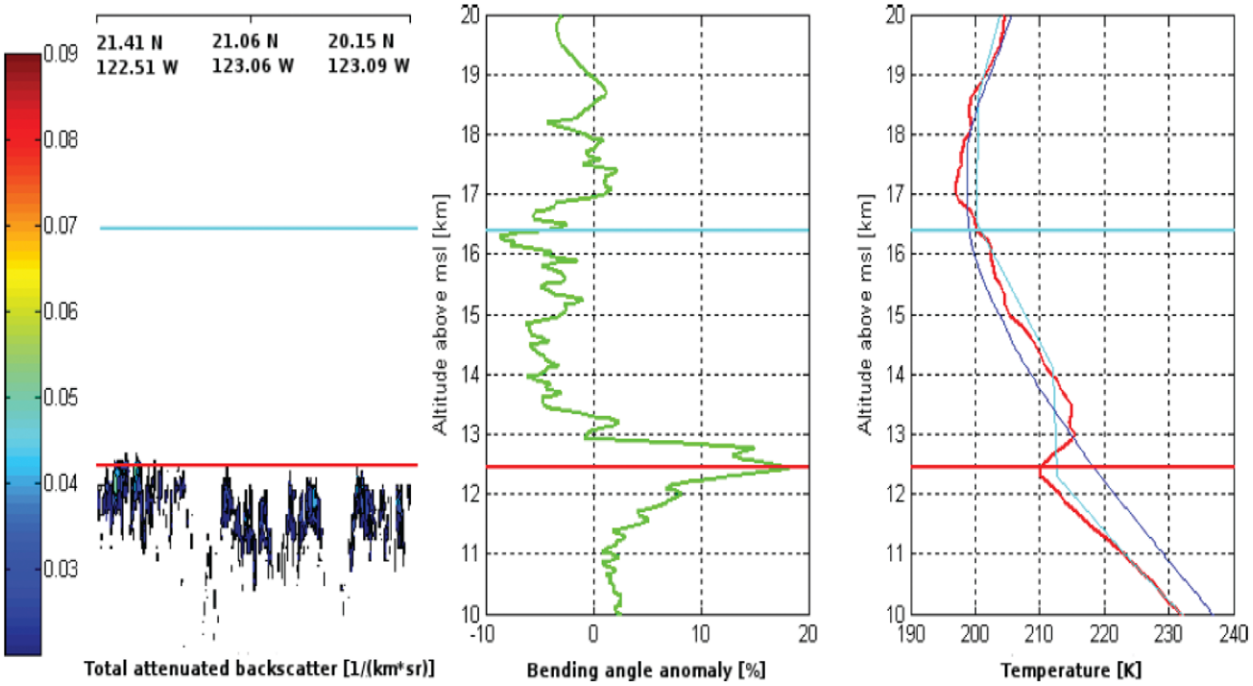


**Fig. 4. Vertical profiles associated with a deep convective system on 2 Feb 2008. (left) The total attenuated backscatter at 532 nm from CALIOP (1008:00 UTC), along the orbit track. (middle) The bending angle anomaly profile (green) and (right) the temperature profiles (red) from GPS RO (0953:00 UTC), the ECMWF analysis (cyan), and the climatology (blue) during the storm. The altitude of the lapse-rate tropopause (horizontal cyan line) and the altitude of the coldest point and the bending angle anomaly spike (horizontal red line) are also presented (adapted from Fig. 3 in Biondi et al. 2012).**

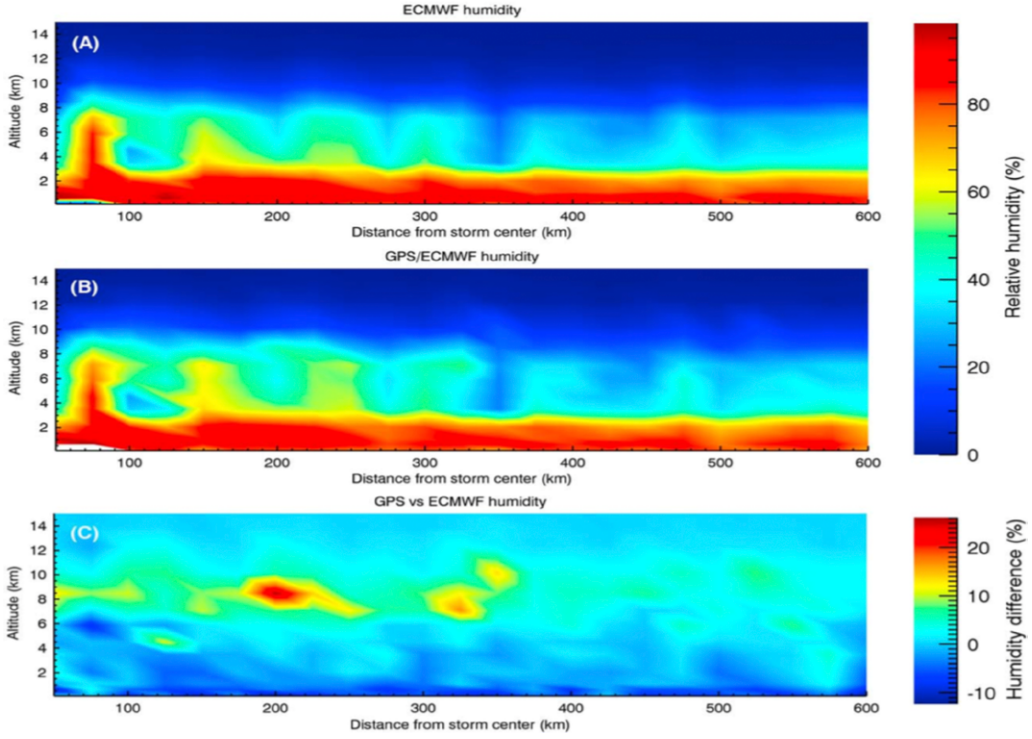


**Fig. 5. Composite (2002–10) tropical cyclone relative humidity (RH) as a function of radial distance from the storm center and altitude. Twenty-five kilometer binned averages of North Atlantic tropical cyclones from (a) ECMWF, (b) RO, and (c) RH fractional difference between the RO and the ECMWF reanalysis (Vergados et al. 2013). Beginning in late 2006 ECMWF began assimilating COSMIC data so the RO and ECMWF analyses are not completely independent.**

COSMIC-2), can contribute to the climatology and study of TC, even though they only resolve horizontally smooth features.

## Impacts of RO on numerical weather prediction

***Global numerical weather prediction.*** It is understood that progress in global NWP is gradual, "resulting from a steady accumulation of scientific knowledge and technological advances over many years" (Bauer et al. 2015). Nevertheless, an important part of this progress has been based on the improved use of existing observations, and the introduction of new observation types. No single observation type provides all the information required for NWP applications, and therefore, the Global Observing System (GOS) attempts to find the right balance of many diverse measurement types. New observations are particularly important for NWP if they provide distinctive information that is not already available from other observations. However, as was pointed out by McNally et al. (2006), modern operational global models and data assimilation are robust, and each observational system contributes only marginally to the overall forecast accuracy. Forecast improvements from a single new observing system are likely to be only a few percent at most. In this context, RO observations have shown a significant positive impact on global NWP forecasts since the launch of COSMIC (Healy 2008, 2013; Aparicio and Deblonde 2008; Poli et al. 2009; Cucurull 2010; Rennie 2010; Bonavita 2014; Bauer et al. 2014). This is because RO measurements complement microwave and infrared sounders by providing information on the temperature, water vapor, and pressure with high accuracy and precision, high vertical resolution in clear and cloudy conditions, and importantly, they can be assimilated without bias correction.

The contribution of RO to global model forecast skill has varied with forecast center and over time as the number of RO observations has changed. A European Centre for Medium-Range Weather Forecasts (ECMWF) study (Cardinali and Healy 2014) for June 2011, when the number of COSMIC RO observations available in near–real time was approximately 2,000 observations per day, showed RO among the top five highest impact observational systems (Fig. 6). This calculation was based on the forecast sensitivity to observation impact (FSOI) diagnostic (Cardinali 2009). The FSOI uses an adjoint approach to estimate how different observing systems reduce a globally integrated scalar cost function, based on the total dry energy errors for 24-h forecasts. In June 2011, RO contributed about 10% to the FSOI, with the contribution peaking in the UTLS region, consistent with earlier theoretical information-content studies (Collard and Healy 2003). Overall, the RO contribution to the FSOI was about the same as AIRS, Infrared Atmospheric Sounding Interferometer (IASI), and aircraft observations during this period

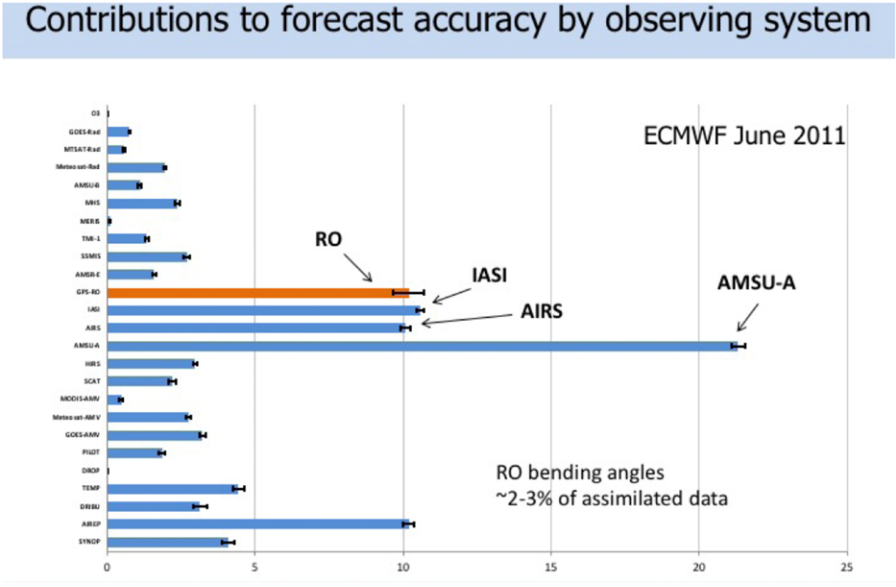


**Fig. 6. Contribution to the forecast sensitivity to observation impact (FSOI) by all the observing systems used by the ECMWF in June 2011. The RO contribution to the FSOI was comparable to AIRS, IASI, and aircraft measurements for this period (Cardinali and Healy 2014).**

(Fig. 6), despite RO bending angles only representing around 4% of the data assimilated into the NWP system. Unsurprisingly, as the COSMIC mission exceeded its planned lifetime, and satellites in the constellation began to fail, the total number of COSMIC RO observations available for operations has decreased steadily. It is currently (late 2018) around 300 COSMIC occultation profiles per day. The impact of this reduction of COSMIC measurements has been partially mitigated through the operational assimilation of RO measurements from the European Organisation of the Exploitation of Meteorological Satellites (EUMETSAT)'s *MetOp-A* and *MetOp-B* satellites (von Engeln et al. 2009) now providing 1,200–1,300 profiles per day, RO measurements from *KOMPSAT-5* providing around 200 occultation profiles per day, and, more recently, RO measurements from the Chinese *Fengyun-3C* satellite providing 300 profiles per day. Nevertheless, the ECMWF computations of the FSOI diagnostic now suggest that the overall RO contribution has fallen from 10% in 2011 to around 5% (see Fig. 1 in Geer et al. 2017). This reduction is partly from the loss of the COSMIC measurements, but also as a result of assimilating more high-resolution infrared radiance information during this period, and the progressively better treatment of microwave radiances within an "all sky" framework (Geer et al. 2017).

In addition to reducing the random errors in the NWP forecasts, the ability to assimilate RO observations without bias correction makes them "anchor measurements" in both NWP and climate reanalysis systems. Anchor measurements prevent the model state from drifting toward its own biased climate in a cycling, data assimilation/variational bias correction (VarBC) system (Dee 2005; Healy et al. 2005; Healy and Thépaut 2006; Healy 2008; Poli et al. 2010; Bauer et al. 2014; Cucurull et al. 2014; Bonavita 2014). This anchoring property increases the impact of the infrared (IR) and microwave sounding systems (Aparicio and Laroche 2015), by constraining the bias corrections applied to the assimilated radiances. Eyre (2016) has also shown that the number of anchor measurement should increase as the number of radiances that require bias correction increases. RO observations can also contribute more directly to the identification of biases in the passive IR and microwave sounding systems, for example, Ho et al. (2009a, 2014) and Zou et al. (2014).

***Impact of RO on regional numerical weather prediction.*** Although it is more difficult to determine the impact of individual observation systems on regional models because of the dominant impact of the specified lateral boundary conditions (Anthes et al. 1985), several studies have shown a positive impact of RO observations on regional model forecasts. For example, Chen et al. (2014) showed a significant improvement in a Weather Research and Forecasting (WRF) Model forecast of an intense synoptic-scale storm that occurred over the Southern Ocean in December 2007. The assimilation of RO data produced an improvement in the large-scale circulation, temperature and water vapor fields, which in turn produced a better track and intensity forecast of the cyclone. Yang et al. (2014) showed a positive impact of assimilating RO refractivities and bending angles in a heavy precipitation event over Taiwan in 2008. The effect of assimilating RO observations, particularly bending angles, was to deepen the depth of moist air (Fig. 7), which enhanced the moisture transport and resulted in increasing the model's forecast precipitation, which was a significant improvement compared to observations.

Numerous studies have shown a positive impact of RO observations on TC forecasts of intensity and tracks (Huang et al. 2005; Kueh et al. 2009; Kuo et al. 2009; Liu et al. 2012). Chen et al. (2015) evaluated three hundred twenty-seven 72-h forecasts of 11 Pacific typhoons in 2008–10 with and without assimilation of RO data. The RO observations improved the analyses of the temperature, water vapor and wind fields, as well as the prediction of the western Pacific subtropical high and its associated large-scale circulation. These improvements resulted in an increase of the forecast track accuracy by an average of 12 km at 72 h (Fig. 8), a modest

but statistically significant improvement. Kuo et al. (2016) also showed a dramatic effect on WRF predictions of the genesis of Typhoon Nuri (2008) when RO data were used (Ho et al. 2019).

The improvements in track and intensity forecasts of TC due to RO observations have been largely due to improvements in the analysis and forecasts of the large-scale TC environment rather than improvements in the analysis of the mesoscale storm structure. This is because the number of RO soundings has been too small and the resulting mean horizontal separation of soundings has been too large to produce a significant number of RO sounding within the storms. However, Vergados et al. (2013) showed that RO soundings within the TC were able to produce accurate retrievals of temperature and water vapor, even near the eye, suggesting that with many more soundings in the tropics as with COSMIC-2, RO will contribute significantly to resolving the mesoscale structure of the storms, resulting in improved track and intensity forecasts. Vergados et al. (2014) showed that RO soundings could resolve high-vertical-resolution (100–200 m) structures of temperature in the UTLS region in the vicinity of hurricane eyewalls, and could be used in estimating the intensity of TC. They point out that these measurements are difficult to obtain from IR and MW observations and that these structures are missing in reanalysis data.

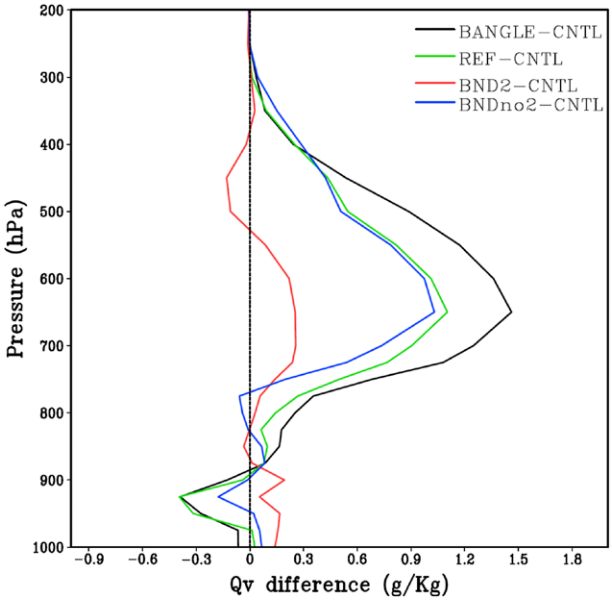


**Fig. 7. Mean difference in water vapor mixing ratio analysis between four experiments assimilating RO observations and a Control (CNTL) experiment in which no RO observations are assimilated. BANGLE assimilates bending angles at all levels in the model. BND2 assimilates RO observations only below 2 km. BNDno2 assimilates RO observations only between 2 and 5 km. REF assimilates RO refractivity (Fig. 15 of Yang et al. 2014).**

***Outstanding issues with assimilation of RO data for NWP.*** Some of the outstanding issues in the assimilation of RO data include whether to assimilate bending angles, refractivity, or other data products of RO such as excess phase, choice of forward observation operators, and characterization of RO errors and quality control.

RO observations of refractivity are derived from bending angles using an Abel transform under the assumption of spherical symmetry (horizontal homogeneity in the region of the observation). In theory, assimilation of bending angles should be superior to assimilation of refractivity. Because bending angles are a higher-level data product, the error characteristics are simpler and they are less sensitive to the assumption of spherical symmetry (Eyre1994). In addition, assimilating refractivity also requires the use of climatology in the upper stratosphere and above to compute the Abel transform. The refractivity values also suffer a negative bias under conditions of superrefraction, which often occurs in the tropical and subtropical boundary layer. Therefore, most operational global NWP centers, including ECMWF, Fleet Numerical Meteorology and Oceanography

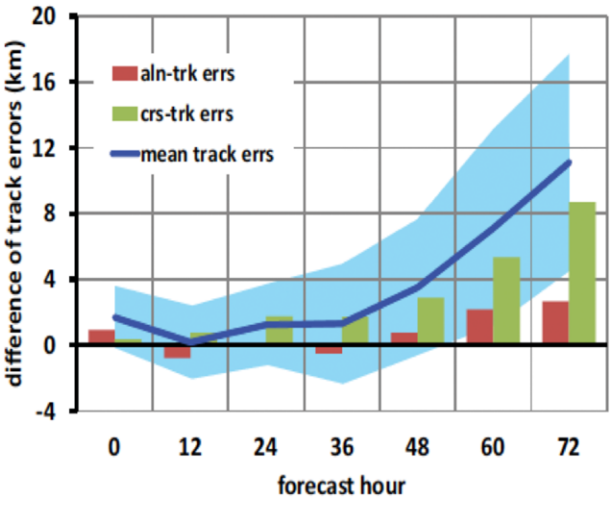


**Fig. 8. Difference in track errors associated with no-RO forecast (PNG) and forecasts with RO (PWG). A positive number means that the RO forecasts have less error (Chen et al. 2015).**

Center (FNMOC), the Met Office, and National Centers for Environmental Prediction (NCEP), assimilate bending angles.

However, assimilation of bending angles has its own challenges. Compared to refractivity, bending angle data have more significant small-scale vertical variability (~100 m scales near surface up to ~400 m scales in the upper troposphere) because the Abel transform filters them out in refractivity space. Many current NWP models do not have sufficient vertical resolution to resolve these small scales, and so filtering of the observed bending angles may be necessary (Gilpin et al. 2019). Alternately, the assumed bending angle error statistics should account for these small-scale unrepresentative structures. The calculation of bending angles in NWP models also requires that the models have high tops (i.e., 60 to 80 km). For lower model tops (e.g., 20 km), typical of many limited-area models, refractivity must be assimilated.

A forward model maps the NWP model state (temperature, water vapor, and pressure) to observation space (bending angle or refractivity). Both 1D and 2D forward models are used. The 2D models account for variations in atmospheric properties in the vertical along the ray path (occultation plane) and are therefore theoretically more accurate, but at a higher computational cost (Healy et al. 2007; Ma et al. 2009; Healy 2014).

Several studies have investigated the potential benefits of 2D refractivity and bending angle operators in RO data assimilation for hurricane analyses and forecasts (Sokolovskiy et al. 2005; Liu et al. 2012). In a simulation of Hurricane Katrina (2005), Ma et al. (2009) showed that the use of a nonlocal excess phase operator produced a more accurate analysis in regions of strong horizontal gradients.

To assimilate RO observations effectively in NWP systems, it is necessary to have a good estimate of the observation error statistics, and to have quality control (QC) procedures to identify and remove measurements with errors that are not consistent with the assumed error statistics. The assumed error statistics and correlations determine the influence, or weight, given to each observation during the assimilation process. The weighting is inversely proportional to the assumed error covariance. The covariance matrix of the combined observation/representation/forward model errors can be estimated from the departures from the observation values and their corresponding background and analysis values (Desroziers et al. 2005; Poli et al. 2009). The NCEP Gridpoint Statistical Interpolation analysis system (GSI) follows this approach for estimating the error statistics (Cucurull et al. 2013). Other operational data assimilation systems use a simpler statistical approach for specifying the error variances (Kuo et al. 2004). For example, ECMWF currently uses a global error statistical model for all RO measurements (Poli et al. 2010). The standard deviation of the error is specified as a percentage of the observed bending angle, where the percentage decreases linearly with impact height, from 20% at the surface to 1.25% at 10 km.

In the moisture-rich lower tropical troposphere, the error characteristics of RO observations varies substantially because of the large horizontal and vertical variability of water vapor. Overall, the operational NWP centers have probably tended to be conservative in estimating the error variance of RO observations, because of increased errors associated with superrefraction in some, but not all, of the RO observations. In theory, therefore, it would be better to vary the weighting of individual RO observations based on their particular accuracy, if the accuracy of each observation can be estimated. Recently, H. Liu et al. (2018) developed a QC method of estimating the accuracy of individual RO observations based on the local spectral width (LSW), which is strongly correlated with the RO retrieval. RO refractivity profiles are truncated where LSW first become larger than the given threshold. H. Liu et al. (2018) found small net improvements in the temperature, water vapor and wind forecasts using the LSW-based QC. Overall these initial results are promising, but they will need to be refined and evaluated with the latest NWP systems, which now include flow-dependent background error statistics.

Atmospheric refractivity profiles can also be observed using airborne radio occulation (see "Airborne radio occultation" sidebar).

### Climate

RO is the only self-calibrated satellite remote sensing technique whose raw measurements can be traced to International System of Units of time (Goody et al. 1998; Ohring 2007; Ho et al. 2010a). RO measurements are well suited for climate monitoring because they (i) have no significant mission-dependent biases above 5 km (Hajj et al. 2004; Ho et al. 2010a,b, 2014; Schreiner et al. 2011), (ii) are of high precision and accuracy (Foelsche et al. 2009; Ho et al. 2009a,b, 2012; Anthes 2011), and (iii) are minimally affected by clouds and precipitation (Ho et al. 2018). Thus, RO data can serve as benchmark datasets (Ho et al. 2007, 2009b; Steiner et al. 2013; Dee et al. 2011) to study atmospheric variability (e.g., Randel et al. 2003; Schmidt

## Airborne radio occultation

Although not directly related to the subject of this paper, we wanted to mention the exciting new technology for using radio occultation to observe the atmosphere using a GPS receiver on aircraft. Haase et al. (2014) describe the first results from an airborne RO (ARO) system using the GNSS Instrument System for Multistatic and Occultation Sensing (GISMOS). The technique is illustrated in Fig. SB1. ARO offers the advantages and opportunities of making targeted RO observations in atmospheric regions of interest, such as tropical cyclones.

The GISMOS was tested during the 2010 Pre-Depression Investigation of Cloud Systems in the Tropics (PREDICT) on the NSF–NCAR Gulfstream-V aircraft, flying at an altitude of ~14 km. At ~1140 UTC 13 September 2010, a GPS satellite set beyond the horizon, producing an occultation. The highest tangent point of the ray path was located at the aircraft position. It drifted 327 km as it decreased to progressively lower heights. Thus, the retrieved refractivity profile is slanted along the direction of the tangent point drift (as is the case with spaceborne RO).

Haase et al. (2014) describe the method for retrieving the refractivity from the excess Doppler shift. The retrieved profile is shown in Fig. SB2 along with a profile computed from a nearby dropsonde, which was released at 1324 UTC approximately 25 km from the deepest tangent point of the RO profile. The difference in refractivity is less than 2% at all levels, and this agreement is comparable to the accuracy of COSMIC RO profiles in the middle and lower troposphere.

Murphy et al. (2015) compared 21 ARO soundings from the PREDICT experiment to dropsondes and the ERA-Interim reanalysis (Dee et al. 2011). They showed that the standard deviation of the differences of the ARO refractivities from the refractivities from the dropsondes and reanalysis was less than 1.5% and 2%, respectively. Chen et al. (2018) demonstrated a positive impact of assimilating these ARO profiles in 3D-Var data assimilation experiments using the WRF Model. They assimilated both local refractivity and nonlocal excess phase, which accounts for the integrated horizontal sampling along the ray path. They found that assimilating the excess phase produced better results compared to assimilating refractivities, and resulted in a decrease of the error in TC Karl's minimum sea level pressure by 43%.

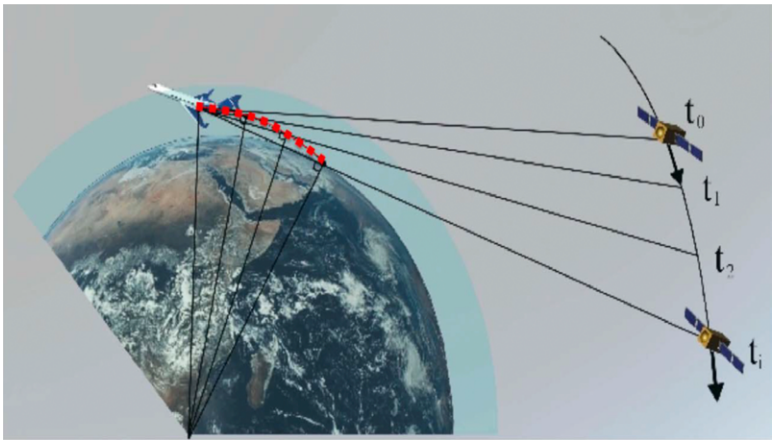


**Fig. SB1. Illustration of the airborne RO geometry (Haase et al. 2014).**

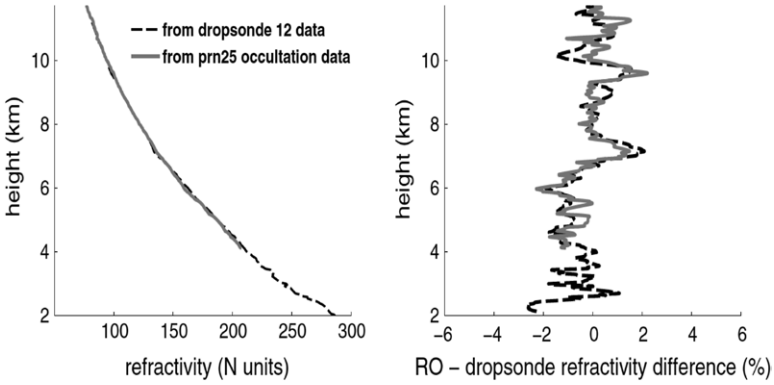


**Fig. SB2. (left) RO refractivity profile obtained from the G-V aircraft compared to the refractivity from a nearby dropsonde. (right) Difference between the RO and dropsonde refractivity (Haase et al. 2014, their Fig. 3).**

et al. 2005; Scherllin-Pirscher et al. 2012; Wilhelmsen et al. 2018) and climate trends (Ho et al. 2009b; Lackner et al. 2011; Steiner et al. 2011, 2013). Dense RO sampling through all local times has also allowed quantification of the diurnal temperature cycle and its seasonal evolution in the upper troposphere and stratosphere (Zeng et al. 2008; Pirscher et al. 2010; Xie et al. 2010a).

***Detection of planetary boundary layer height and stratocumulus cloud-top height.*** Many studies (e.g., Sokolovskiy et al. 2006, 2010a; Ao et al. 2012a; Xie et al. 2006, 2012; Guo et al. 2011; Ho et al. 2015) have demonstrated that the high vertical resolution of RO refractivity and bending angle profiles can detect structures with sharp changes of vertical gradient of density such as marine boundary layer height (MBLH). Ho et al. (2015) compared the COSMIC-derived MBLH collocated with those estimated from lidar cloud measurements from the Cloud–Aerosol Lidar with Orthogonal Polarization (CALIOP) instrument on board the *Cloud–Aerosol Lidar and Infrared Pathfinder Satellite Observations (CALIPSO)* satellite. Figure 9 shows that the three-month running means from September 2007 to March 2010 for the MBLH derived from COSMIC refractivity and bending angle profiles ($MBLH_N$, green, and $MBLH_{BA}$, blue) closely follow the seasonal variation of $MBLH_{CALIOP}$ (orange). The MBLH derived from the minimum in vertical refractivity gradient of ERA-Interim is observed to have a low bias (Fig. 9, red line). This study also suggests that ERA MBLH altitudes are biased low, as also found by Xie et al. (2012).

***Detection of tropopause height.*** The tropopause identifies the transition from the troposphere to stratosphere, and plays a key role in dynamical variability and exchange of trace gases between these regions. It has also been identified as a metric for climate change (Santer et al. 2003). The high vertical resolution of RO temperature profiles makes them ideal to quantify the climatological structure and variability of the tropopause, which helps understanding of the exchange of trace species (such as water vapor and ozone) between the troposphere and stratosphere (Randel et al. 2003; Schmidt et al. 2005, 2008; Lewis 2009; Grise et al. 2010; Kim and Son 2012; Zeng et al. 2012; Rieckh et al. 2014; Randel and Wu 2015). Novel diagnostics of tropopause behavior with RO data include identifying the occurrence of double tropopauses (Schmidt et al. 2006; Randel et al. 2007a) and quantifying characteristics of the extratropical tropopause inversion layer (Randel et al. 2007b; Schmidt et al. 2010; Randel and Wu 2010). Many studies (e.g., Seidel et al. 2008; Birner 2010; Ao and Hajj 2013; Davis and Birner 2013) used the decadal increase of tropopause height detected by RO data as evidence of a widening of the tropical belt resulting from climate change.

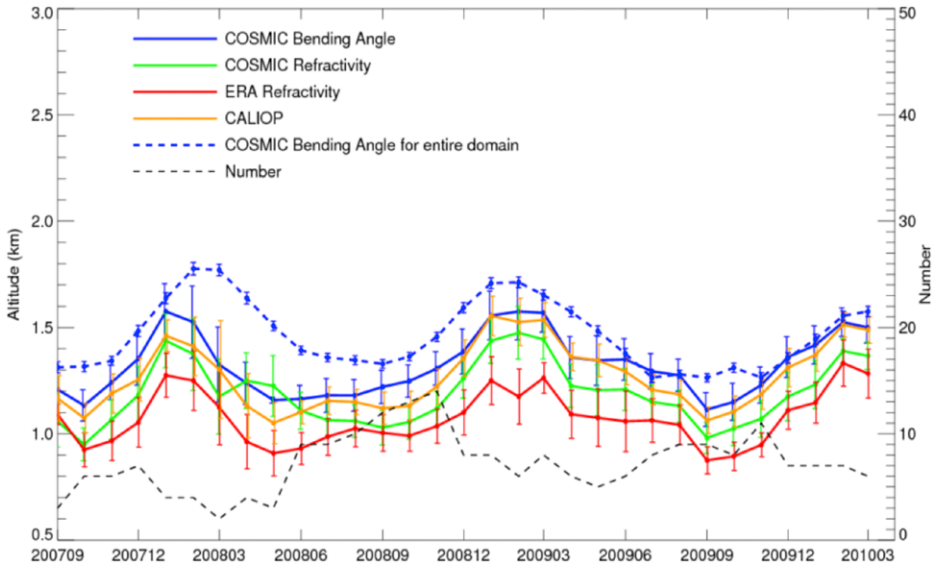


**Fig. 9. Three-month running means from September 2007 to March 2010 for the MBLH computed from RO bending angles and refractivity, the ERA-Interim refractivity profiles, $MBLH_{CALIOP}$, and the $MBLH_{BA}$ from the entire VOCALS region (Fig. 12 of Ho et al. 2015).**

***Water vapor profiles and total precipitable water.*** In the troposphere, RO refractivity is a function of temperature and water vapor. A 1D-Var algorithm is used in CDAAC (http://cosmic-io.cosmic.ucar.edu/cdaac/doc/documents/1dvar.pdf) to derive temperature and water vapor profiles using the ERA-Interim reanalysis as a priori information (Zeng et al. 2012). RO refractivity is sensitive to water vapor errors in the lower troposphere, and is less sensitive to temperature errors (Ware et al. 1996). Thus for a given observed refractivity and a direct retrieval of water vapor using an independent estimate of temperature, a temperature error of 1 K will introduce less than 0.25 g $kg^{-1}$ of water vapor error in the lower troposphere. Kursinski and Gebhardt (2014) estimated one-sigma random uncertainties of 0.14 g $kg^{-1}$ at 346 hPa increasing to 0.39 g $kg^{-1}$ at 725 hPa (their Table 2). Neiman et al. (2008) showed that the retrieved 1D-Var water vapor profiles are not very sensitive to the first guess water vapor profiles in the 1D-Var retrieval that they used. Differences between the retrieved specific humidity values using the GFS and ECMWF model fields were generally less than 1 g $kg^{-1}$, which were significantly smaller than the differences between the GFS and ECMWF specific humidities themselves (Fig. 14 in Neiman et al. 2008). Thus, RO observations are useful to quantify the moisture distribution within and outside clouds in the middle and lower troposphere (below about 400 hPa), including regions with extremely moist and dry layers such as the subtropical Pacific (Rieckh et al. 2017, 2018) except for superrefraction regions dominated by sharp boundary layer over oceans (Ho et al. 2015). Steiner et al. (2018) demonstrated the use of RO for the evaluation of temperature and humidity in climate models in tropical convection regimes.

COSMIC-derived total precipitable water (TPW) estimates have been validated by using ground-based GPS. Ho et al. (2010a) showed that the mean global difference between ground-based and COSMIC TPW is about −0.2 mm with a standard deviation of 2.7 mm. This is consistent with comparisons from Teng et al. (2013) and Huang et al. (2013). Figure 10 depicts global average TPW anomalies (1981–2010 reference period) for oceans (Fig. 10a) and land (Fig. 10b) for COSMIC and ground-based GPS observations (over land only) and three reanalyses averaged over 60°S to 60°N. The TPW anomaly time series show maxima in 1983/84, 1987/88, 1997/98, 2009/10, and late 2015, associated with El Niño events. Over land and oceans the observations and reanalyses show an increase in TPW over this time period.

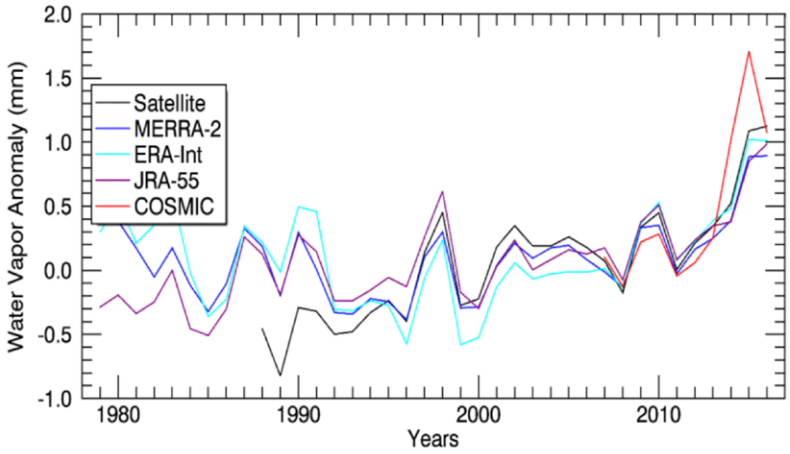


(a) Oceans

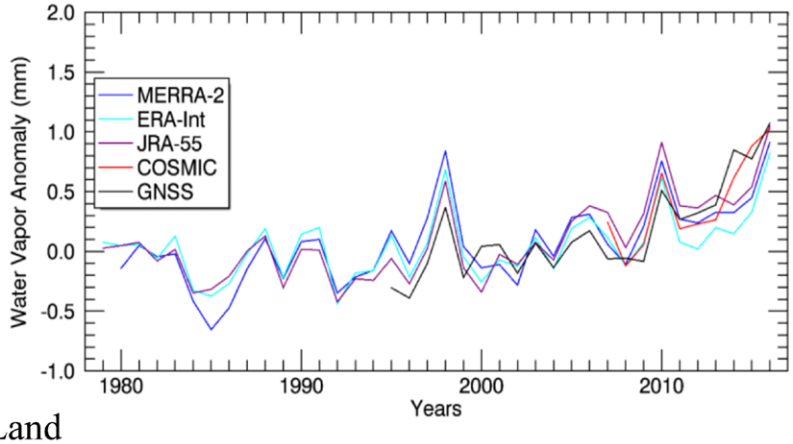


(b) Land

**Fig. 10. Global mean total precipitable water vapor annual anomalies for (a) ocean only and (b) land only for observations and reanalysis averaged over 60°S to 60°N. The shorter time series have been adjusted so that there is zero mean difference relative to the mean of the three reanalyses over the 2006–14 period (constructed from same data as in Mears et al. 2017, their Fig. 2.16).**

***On-orbit references to calibrate and correct satellite data and in situ data.*** Recent long-term variations of atmospheric vertical thermal distributions are mainly constructed from passive satellite microwave [i.e., Microwave Sounding Unit (MSU) and the Advanced Microwave Sounding Unit (AMSU)] and infrared sounders. However, because these instruments are not designed for climate monitoring, the intersatellite biases can be on the order of 1 K and show variability ranging from a few tenths to several kelvin.

Because the six COSMIC satellites sampled all local time periods globally, they could identify possible radiative biases of microwave measurements in the lower stratosphere (from 8 to 30 km). Comparisons of lower stratospheric temperatures revealed differences between the microwave record and RO (Ho et al. 2007; Steiner et al. 2007; Ladstädter et al. 2011; Dee 2011). Ho et al. (2007, 2009a) demonstrated that because COSMIC data, unlike MSU/AMSU data, do not contain orbit drift errors and are not affected by on-orbit heating and cooling of the satellite components, they are useful for identifying the AMSU time/location-dependent biases for different missions.

***Correction of radiosonde systematic temperature biases.*** Radiosonde observations (raobs) have provided global in situ temperature, moisture, and wind measurements in the troposphere and lower stratosphere since 1958. However, because the quality of raob data varies with sensor types and altitude, it is difficult to use historical raob data to construct consistent temperature climate data records (Thorne et al. 2011; Seidel et al. 2011). Reanalyses, such as those discussed in the "Impact of radio occultation on climate reanalyses" sidebar, typically adjust these raob data to remove estimated biases prior to assimilation of the data.

Several studies have demonstrated that RO observations can be used as a reference to identify raob sensor-dependent biases as well as biases due to radiative effects (Kuo et al. 2004; He et al. 2009; Sun et al. 2010, 2013). Ladstädter et al. (2015) compared RO observations with high quality radiosondes (Vaisala RS90/92) from 2002 to 2013 as well as the Global Climate Observing System (GCOS) Reference Upper Air Network (GRUAN) available since 2009. Although there was overall good agreement in all three datasets, there were larger temperature differences in the stratosphere above 30 hPa and day/night comparisons with GRUAN data showed small deviations likely related to a warm bias of the radiosonde data at high altitudes.

Figure 11 depicts the mean temperature biases at 50 hPa as a function of solar zenith angle (SZA) for Sippican over United States minus RO (Fig. 11a), VIZ-B2 over United States minus RO (Fig. 11b), AVK Russian minus RO (Fig. 11c), and Shanghai minus RO (Fig. 11d). The different sensors contain different systematic biases relative to those of collocated RO temperature during the daytime and nighttime. The VIZ-B2 sondes have a large warm bias (as high as 2.0 K) during daytime and a cold bias (as low as −1.0 K) at night. The nighttime bias of this particular type of radiosonde is atypical, in that the other types shown in Fig. 11 have nighttime biases of at most a few tenths of a kelvin, and biases of a similar order may be inferred from an extensive intercomparison of radiosonde types reported by Nash et al. (2011). Nevertheless, while Fig. 11 shows the AVK instrument to have nighttime biases close to zero, this instrument has a bias from about 0.7 to 1.1 K in the daytime. Because the quality of RO temperature is not affected by sunlight, the small but obvious geographic-dependent biases are most likely due to the residual radiation correction for these sensor types. Using a similar approach, Ho et al. (2017) also characterized (i) SZA-dependent temperature errors due to incomplete radiation correction, (ii) temperature biases due to change of radiation correction over different geographical regions, and (iii) the interseasonal and interannual variability of these temperature biases.

***Identifying water vapor biases from microwave imager below clouds.*** Ho et al. (2010b) demonstrated that RO-derived water vapor profiles can be used to distinguish systematic

## Impact of radio occultation on climate reanalyses

RO measurements have had a significant impact on upper-tropospheric and lower/middle-stratospheric temperature reanalyses from 2006 onward since COSMIC measurements have been assimilated. This is primarily, as noted the "Impacts of RO on numerical weather prediction" section, because RO is an "anchor" measurement. Poli et al. (2010) described the use of CHAMP and COSMIC measurements in the ERA-Interim reanalysis. They found that the assimilation of COSMIC measurements from 2006 resulted in a warmer tropopause and lower stratospheric analysis globally by about 0.1–0.2 K, and reduced both ERA-Interim background-forecast and analysis biases with respect to radiosonde temperature measurements that had been independently adjusted to reduce their biases. The assimilation of CHAMP data alone was not sufficient to constrain the temperature biases. In the context of estimating low-frequency variability and trends, Simmons et al. (2014) confirmed that RO improved the fit to bias-adjusted radiosonde temperatures in a longer time series. They also showed that for ERA-Interim, RO modified the bias corrections applied to satellite radiances, including HIRS channel 2 and AMSU-A channel 10, and reduced a quite severe cold bias of around 0.5 K or more at the tropical tropopause, as can be seen in Fig. SB3.

More recently, Long et al. (2017) found that "GPSRO provides an anchor that drives the reanalyses to closer agreement in the middle and lower stratosphere." This conclusion was based on computing the spread (standard deviation) of the global, annual average of four reanalyses mapped to MSU channel 4 brightness temperature space, which is a relatively coarse, vertically integrated measure. However, Fig. SB3 also shows that in 2006 there was a clear convergence of the tropical temperature at 100 hPa, in the reanalyses that assimilate RO [ERA-Interim, JRA-55 (Kobayashi et al. 2015), MERRA-2 (Gelaro et al. 2017), and ERA5 (Hersbach and Dee 2016; Hersbach et al. 2018)]. However, MERRA—which did not assimilate RO and can be inferred from Fig. SB3 to have a warm tropical tropopause bias (along with JRA-55 prior to 2006)—did not converge. The details of the assimilation strategy and the products ingested (e.g., the use of reprocessed or operational RO data; use of data from other missions) differ among the reanalysis systems that assimilate RO, but they all share the large increase in usage of RO during 2006 with the availability of COSMIC.

An interesting, indirect impact of assimilating RO data on the ERA-Interim stratospheric water vapor reanalysis is suggested by recent results presented by Davis et al. (2017). They found a distinct positive shift in the ERA-Interim tropical stratospheric water vapor anomalies around 2007 (see their Fig. 15f). The RO data do not provide any direct information on stratospheric water vapor, but they do reduce the cold bias at the ERA-Interim tropical tropopause, and this modifies the freeze-drying (dehydration) process in the tropical tropopause layer, which determines the water vapor entering the stratosphere (Brewer 1949). Further work is required here, but it appears to illustrate how assimilating data with a dynamical forecast model can increase the effective information content of the observations.

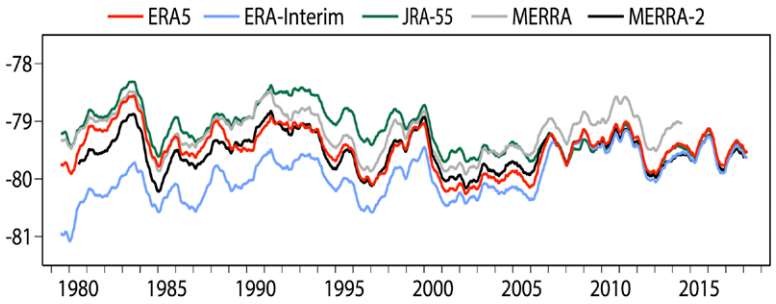


**Fig. SB3. Twelve-month running mean temperature (°C) at 100 hPa averaged over the tropics (20°S to 20°N) from five global reanalyses. All assimilate GPS radio occultation (RO) data after 2006 except MERRA (light gray line). RO observations from COSMIC are available from April 2006 to end of period (September 2018). Other RO missions from which data are assimilated in at least one of these reanalyses include CHAMP, MetOp, *GRACE-A*, *SAC-C*, *TerraSAR-X*, *FY-3C*, and *TanDEM-X*. From the time COSMIC RO observations begin to be assimilated, the average temperatures of the four reanalyses that assimilate these data converge while the MERRA temperatures remain significantly higher.**

biases among humidity sensors. Global TPW can be derived from satellite visible, infrared, and microwave (MW) sensors (i.e., Wentz and Spencer 1998; Fetzer et al. 2006; John and Soden 2007; Fetzer et al. 2008; Noël et al. 2004). Wentz (2015) concluded that MW imagers are among the few satellite instruments that are able to provide long-term (close to 30 years) all-weather time series of water vapor measurements over the oceans using similar sensors and retrieval techniques. However, many studies (Schluessel and Emery 1990; Wentz and Spencer 1998) also indicated that because MW radiation is significantly affected (absorbed or scattered) by heavy rain, the retrieved MW TPW are less certain under cloudy and precipitating conditions. Wick et al. (2008) were the first to compare SSM/I retrievals of TPW with those from COSMIC. They found close agreement with TPW retrieved from four SSM/I sensors and COSMIC, supporting the validity of both ways of measuring TPW. Small differences were attributed to SSM/I variations with latitude, cloud liquid water content, rain rate, and wind speed. Additional small differences were related to the larger horizontal footprint of the RO observations.

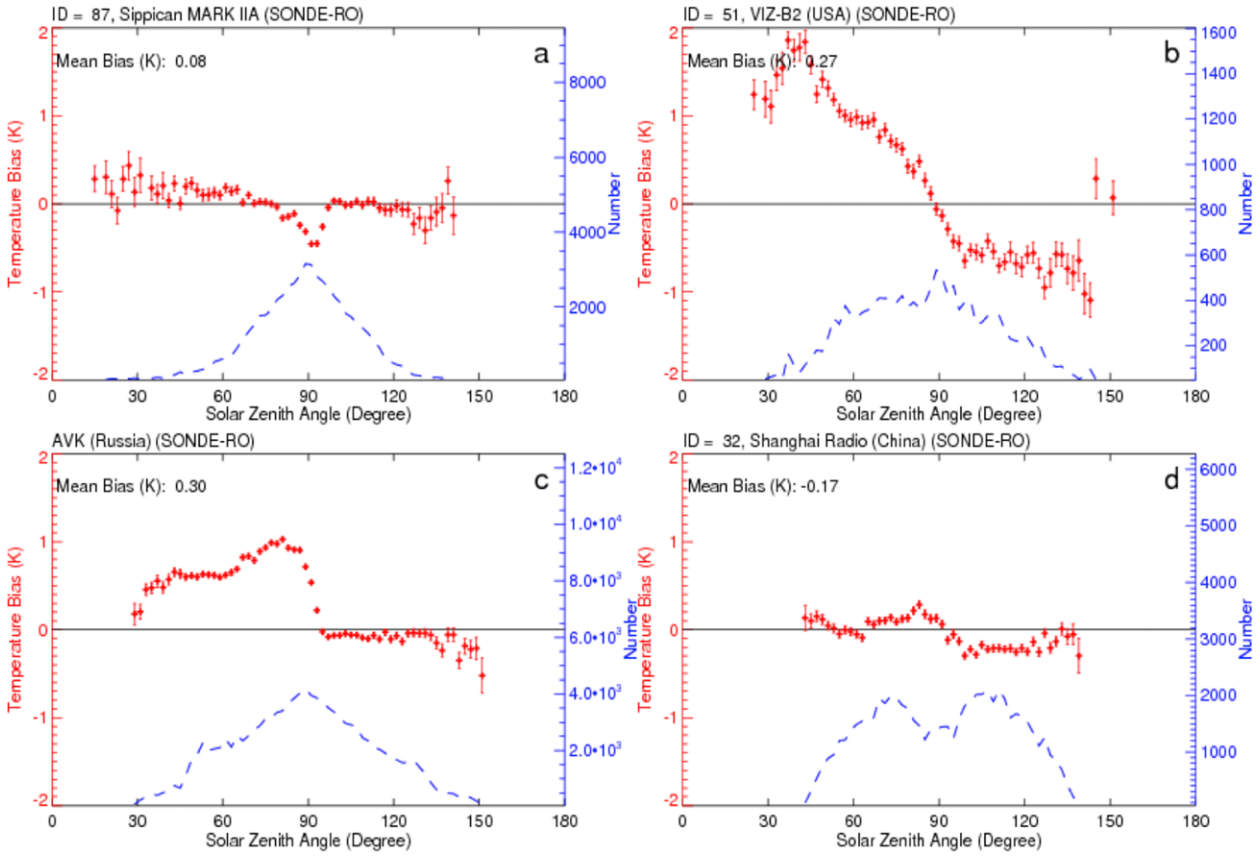


**Fig. 11. The mean temperature biases (radiosonde minus RO) at 50 hPa for solar zenith angle (SZA) ranging from 0° to 180° for (a) Sippican over United States, (b) VIZ-B2 over United States, (c) Russian sonde, and (d) Shanghai radiosondes. Only bins with more than 50 raob–RO pairs are plotted (Ho et al. 2017, their Fig. 8).**

Figure 12 shows TPW scatterplots for the COSMIC and RSS Version 7.0 *F16* SSM/I pairs from June 2006 to December 2013 under different atmospheric conditions (Schröder et al. 2017; see also Ho et al. 2018). Because most of the COSMIC profiles do not penetrate to the surface over oceans, the water vapor profile below the penetration height is interpolated assuming the relative humidity is equal to 80% where the temperature distribution is extrapolated from the temperature of penetration height and surface skin temperature.

Under clear conditions where SSM/I provide high quality TPW products, the TPW bias between SSM/I and COSMIC (i.e., SSM/I–COSMIC) is 0.03 mm with a standard deviation of 1.47 mm. Figure 12b shows that there are positive TPW biases under cloudy conditions, mainly resulting from SSM/I retrieval biases (~0.79 mm). Figure 12d shows that the large SSM/I TPW biases are caused mainly from pixels under precipitation (bias 1.83 mm) although precipitation pixels are approximately less than 6% of the total SSM/I–COSMIC pairs. This result demonstrates the feasibility of using RO TPW values to not only identify, but also to correct those derived from microwave radiometers under cloudy and precipitating conditions.

***Atmospheric blocking.*** The value of using RO observations to analyze global atmospheric blocking was first demonstrated by Brunner et al. (2016) for two major events (Russia in 2010 and Greenland in 2013). RO vertically resolved geopotential height gradients showed a distinct anomalous pattern up to 300 hPa and a pronounced tropopause height increase compared to climatology. Using RO data from 2006 to 2016, Brunner and Steiner (2017) provided a global perspective of blocking. They found that the main blocking regions in the Northern and Southern Hemispheres and seasonal variations are well represented by RO observations, which are particularly useful for insight into the vertical temperature and humidity structures during

blocking, especially in the Southern Hemisphere where other observations are sparse.

## Ionosphere research and applications

The globally distributed profiles of the E- and F-region ionosphere provided by RO have enabled significant advances in ionosphere research and applications. This is especially true in the past 10 years due to the 1,000–2,000 ionosphere profiles per day provided by COSMIC. Yue et al. (2014) provide an overview of the ionosphere observations from COSMIC, and Anthes (2011) summarizes initial scientific results. By providing an unprecedented view of the global ionosphere, the COSMIC observations have led to new understanding of the climatology and variability of the ionosphere. This includes both the large-scale structures, as well as smaller-scale irregularities that can disrupt communications and navigation signals. Upper atmosphere data assimilation models are rapidly developing due to the need to nowcast and forecast the near-Earth space environment, and COSMIC observations have proven to be important for upper atmosphere data assimilation models.

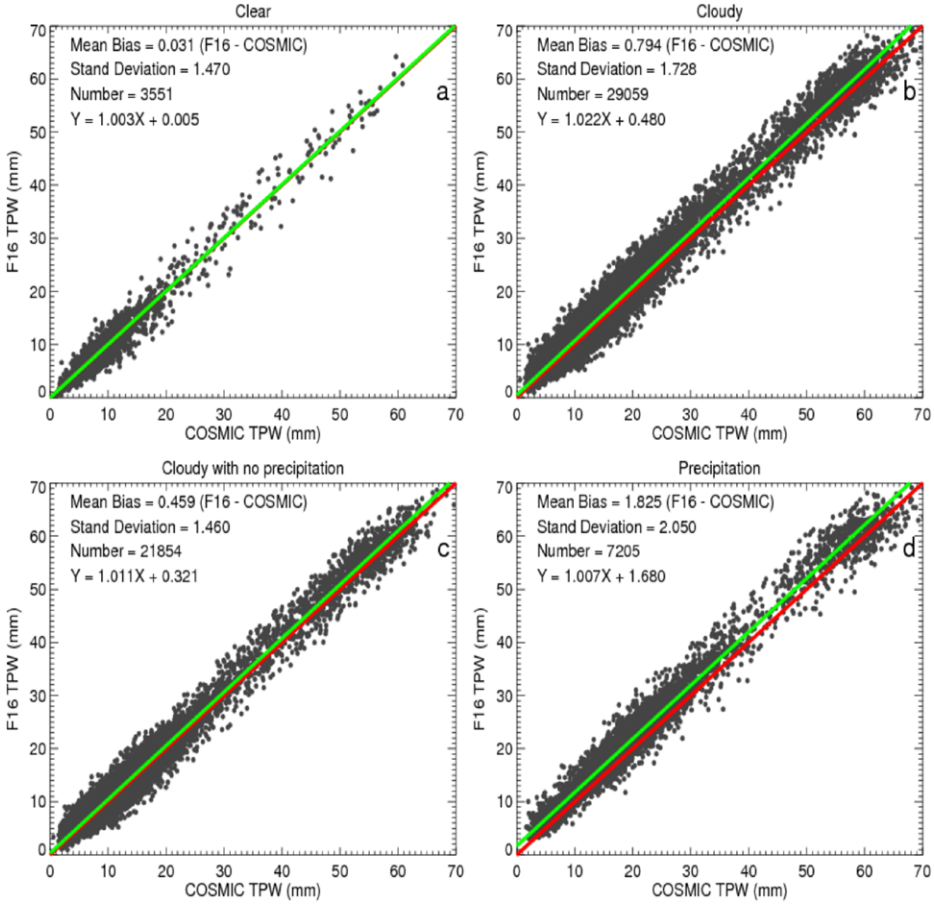


**Fig. 12. Scatterplots for the COSMIC and RSS Version 7.0 *F16* SSM/I vs COSMIC RO pairs under (a) clear, (b) cloudy, (c) cloudy but nonprecipitating, and (d) precipitating conditions (Schröder et al. 2017).**

***Observational studies.*** Through its impact on the vertical distribution of joule heating, the conductivity of the high-latitude ionosphere is important for understanding the distribution of energy input into the upper atmosphere during geomagnetic storms (e.g., Thayer et al. 1995). Despite its importance, the high-latitude conductivity is poorly known due to the difficulty in observing the horizontal and vertical electron density distribution at high latitudes. Sheng et al. (2014) used COSMIC observations to study the high-latitude conductance, and determined the relative importance of the E- and F-region electron density to the total conductance. They found the ratio between the E- and F-region conductivity to be seasonally dependent, more so in the Southern than the Northern Hemisphere. Sheng et al. (2014) further compared the observed conductivities with those from a first principles general circulation model [Thermosphere–Ionosphere–Electrodynamics General Circulation Model (TIE-GCM)], and found that the model significantly underestimates the F-region conductivity, indicating an underestimate of energy deposition in the high-latitude F-region ionosphere.

The COSMIC sampling density is sufficient to observe the latitude, longitude, and local time variability of the ionosphere on time scales as short as roughly one week, providing insight into certain aspects of ionospheric variability. Tulasi Ram et al. (2010a,b) used COSMIC

observations to study the latitude, altitude, and local time dependencies of the ionosphere response to the recurrent geomagnetic activity. The COSMIC observations (Fig. 13) revealed that the ionosphere electron density response to the geomagnetic activity exhibits altitude and latitude dependencies. This gives insights into the physical mechanisms driving the response, and Tulasi Ram et al. (2010a) attributed these differences to the relative importance of changes in ionosphere scale height, neutral composition, particle precipitation, and loss coefficients in different altitude and latitude regions.

Understanding of how the lower atmosphere drives ionospheric variability has also been enabled by COSMIC observations. Sudden stratospheric warming (SSW) events introduce perturbations in the ionosphere that persist for several weeks (e.g., Chau et al. 2012). A number of studies have used COSMIC observations to uncover new aspects of ionospheric variability during SSW events (Jin et al. 2011, 2012; C. H. Lin et al. 2012; J. T. Lin et al. 2012; Lin et al. 2013; Yue et al. 2010a; Oyama et al. 2014; Pedatella et al. 2014; Pedatella and Maute 2015). These studies have benefitted from the global sampling and vertical profiling of the ionosphere to investigate aspects of the SSW response that cannot be obtained through other observations, such as ground-based total electron content (TEC) observations. For example, Fig. 14 (Pedatella and Maute 2015) shows variations in the F-region peak height (hmF2) from COSMIC and Thermosphere–Ionosphere–Mesosphere–Electrodynamics General Circulation Model (TIME-GCM) simulations during the 2009 SSW. Both the observations and model simulations reveal changes in the ionosphere peak height in the midlatitude Southern Hemisphere around the SSW time period (vertical dashed line). These perturbations are reproduced in the model simulations when the atmospheric lunar tide is considered in the simulations. Analysis of the model simulation reveals that these perturbations are related to the influence of the atmospheric lunar tide on thermospheric meridional winds. These results provide observational evidence that perturbations in the Northern Hemisphere stratosphere produce ionosphere–thermosphere variability near 300 km altitude in the Southern Hemisphere.

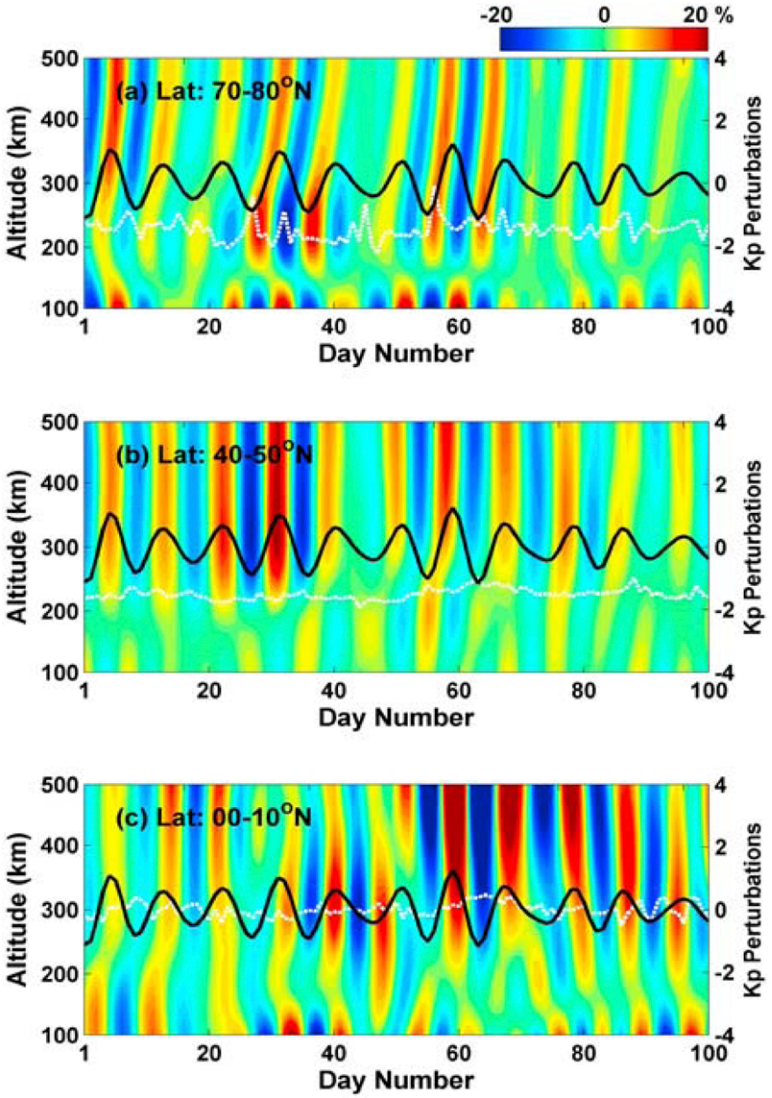


**Fig. 13. Bandpass filtered 9-day perturbations in electron density at (a) high (70°–80°N), (b) middle (40°–50°N), and (c) low (0°–10°N) latitudes as a function of altitude and day. The black curves represent the 9-day bandpass filtered perturbations in the Kp geomagnetic index (Tulasi Ram et al. 2010a).**

In addition to observing the large-scale structures, RO observations provide information about E- and F-region ionosphere irregularities. Carter et al. (2013) used this feature to study the global morphology of F-region ionosphere irregularities. This study provided information

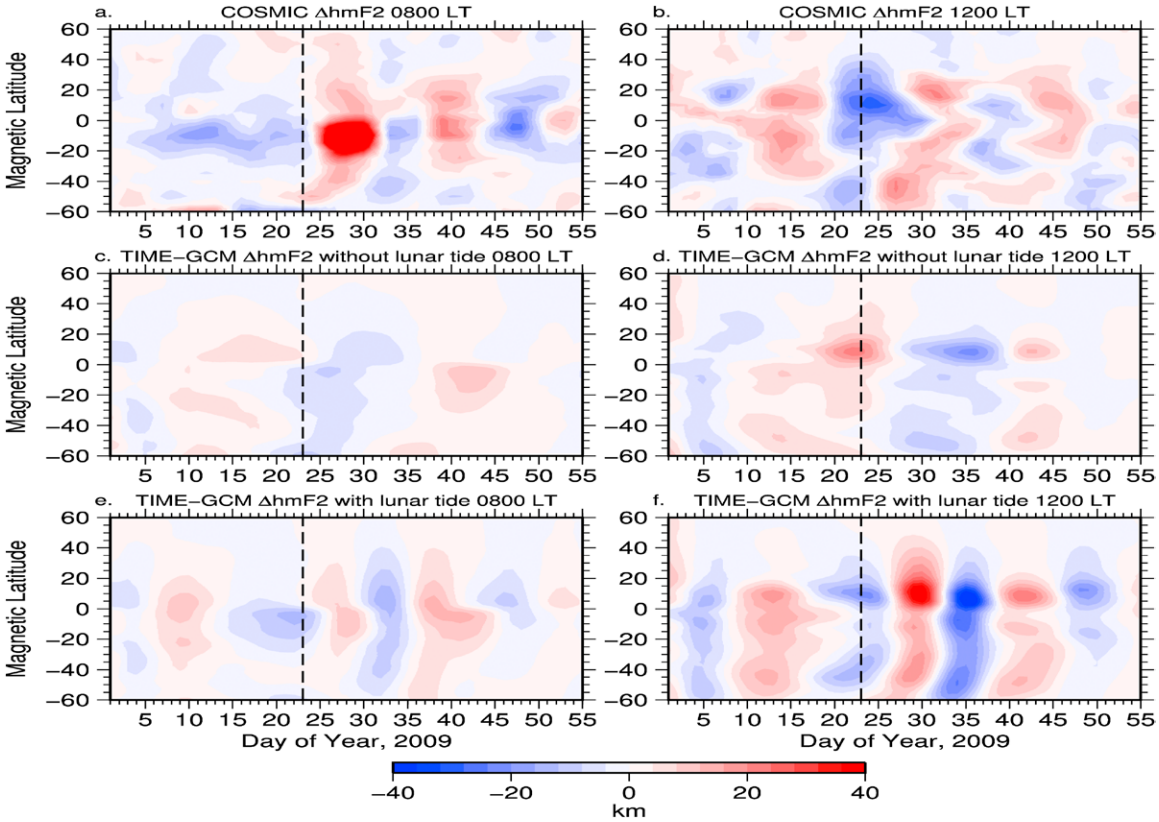


**Fig. 14. Perturbations in COSMIC hmF2 at (a) 0800 and (b) 1200 local time. (c),(d) As in (a),(b), but for the TIME-GCM simulation without the $M_2$ lunar tide. (e),(f) As in (a),(b), but for the TIME-GCM simulation with the $M_2$ lunar tide. Results are the 5-day running mean averaged over all longitudes (Pedatella and Maute 2015).**

on the occurrence of irregularities in regions that are not monitored routinely by ground-based instrumentation. The climatological distribution of F-region irregularities agreed with previous investigations, indicating that RO observations are well suited for studying the global characteristics of F-region irregularities. Carter et al. (2013) additionally found that the solar activity dependence of equatorial F-region irregularity occurrence differs with geographic location, demonstrating the need for prolonged RO observations of the global distribution of ionosphere irregularities. Seif et al. (2017) used COSMIC RO to confirm that sporadic E layers can exist at the geomagnetic equator during daytime, in contrast with prevailing expectation.

Yue et al. (2016) investigated the influence of sporadic E layers and F-region irregularities on the occurrence of cycle slips within the COSMIC precise orbit determination GPS receiver. They found that cycle slips in the E region are primarily due to the occurrence of sporadic E layers (Fig. 15). In contrast, cycle slips that occur in the F region were due to large-scale gradients in the daytime ionosphere. The nighttime F-region cycle slips were attributed to F-region irregularities. A significant finding was that, due to the ionosphere, cycle slips contaminate ~23% of RO observations. Uncorrected cycle slips can influence the RO observations, and this study indicates that understanding the role of the ionosphere and cycle slip occurrence may improve RO data processing and results.

The global nature of the COSMIC ionosphere electron density profiles enabled the first study of the three-dimensional structure of the ionosphere midlatitude trough (Lee et al. 2011). Though prior studies identified basic features of the midlatitude trough, such as being narrow in latitude and extended in longitude, they were limited by insufficient observations, especially in the Southern Hemisphere. Using COSMIC observations, Lee et al. (2011) studied

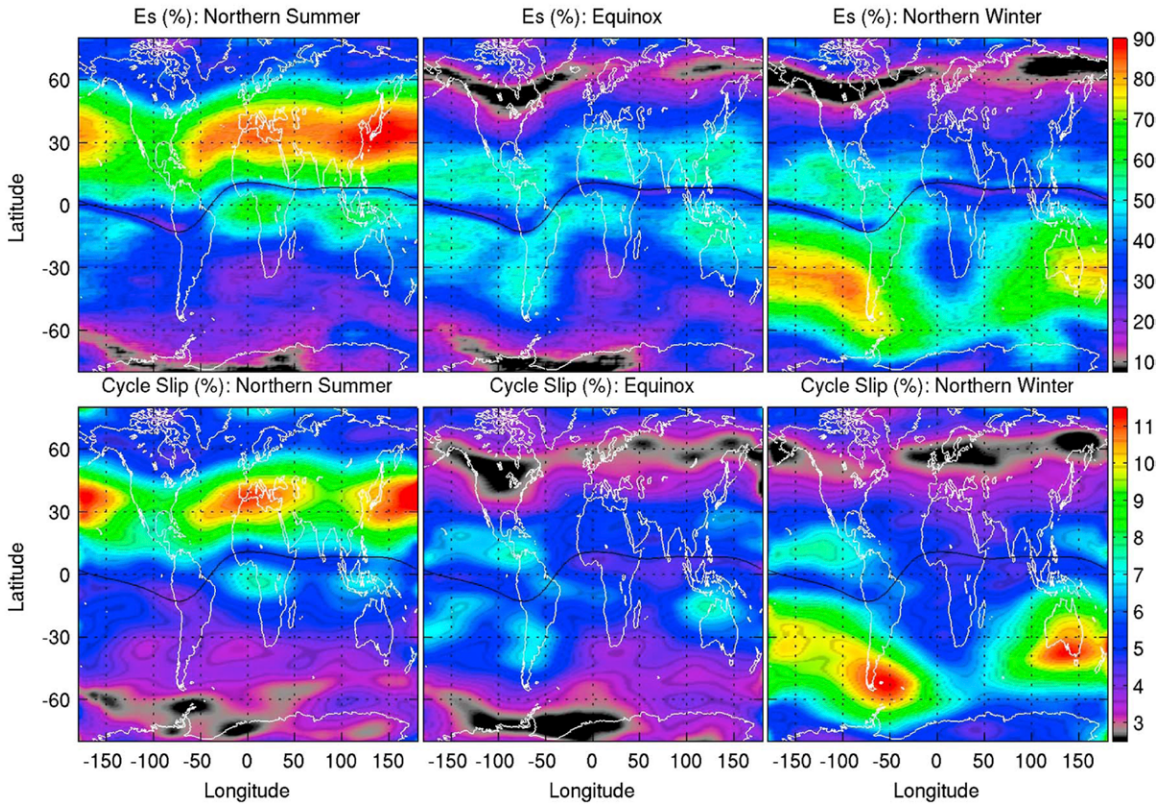


**Fig. 15. Global distribution of the sporadic (top) E-layer occurrence rate and (bottom) cycle slip occurrence rate per occultation in the E region (%). Results are shown for (left) northern summer, (middle) equinox, and (right) northern winter seasons (Yue et al. 2016).**

the climatological features of the midlatitude trough during solar minimum in both the Northern and Southern Hemispheres. Figure 16 illustrates the vertical distribution of electron density during February–April 2008. The midlatitude trough, which is characterized by the depleted regions of electron density around midnight near ±60° magnetic latitude, displays a clear altitude and local time dependence.

***Data assimilation.*** COSMIC observations have been widely adopted for use in ionosphere data assimilation models. This is primarily due to the fact that RO provides information on the ionosphere profile shape as well as providing observations in regions where other ionosphere observations are notoriously sparse, such as over the ocean. Using data denial experiments, the influence of RO observations on the global reconstruction of the ionosphere was investigated by Gardner et al. (2014) and Schunk et al. (2016) in the Utah State University Global Assimilation of Ionospheric Measurements (GAIM) data assimilation model. TEC changes of up to 40% occur due to inclusion of the RO data (Fig. 17). As demonstrated by Schunk et al. (2016) the RO data also introduces large changes to the NmF2 and hmF2, especially over the oceans. Several other data assimilation models have similarly shown the significant impact of the COSMIC observations (Lin et al. 2015; Pedatella et al. 2015).

Although it is a significant driver of ionosphere variability, the thermosphere is difficult to observe directly. By using data assimilation, RO observations have proven to be useful for inferring information about the thermosphere. Using an ensemble Kalman filter approach in a coupled thermosphere–ionosphere general circulation model, Matsuo et al. (2013) found that the assimilation of RO observations is effective for constraining the thermosphere neutral mass density globally. This is due to the abundance of RO observations as well as the correlation between neutral mass density and electron density. The thermosphere neutral

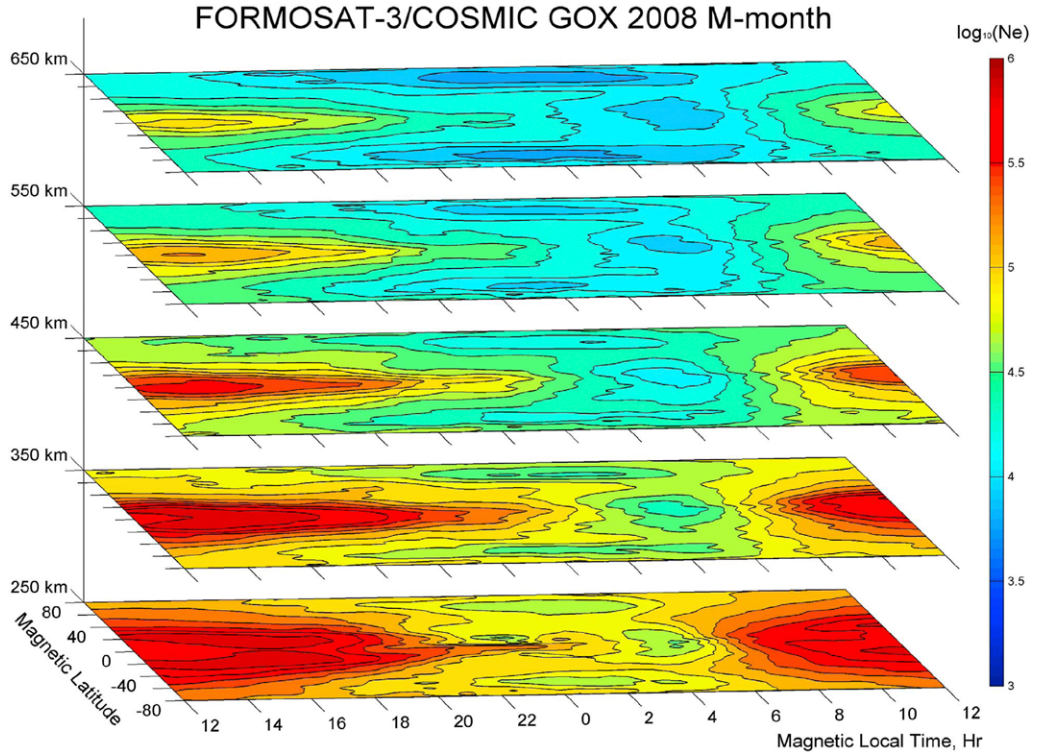


**Fig. 16. Electron density maps at 250, 350, 450, 550, and 650 km altitude in magnetic latitude vs magnetic local time coordinates obtained from COSMIC RO observations during February–April 2008 (Lee et al. 2011).**

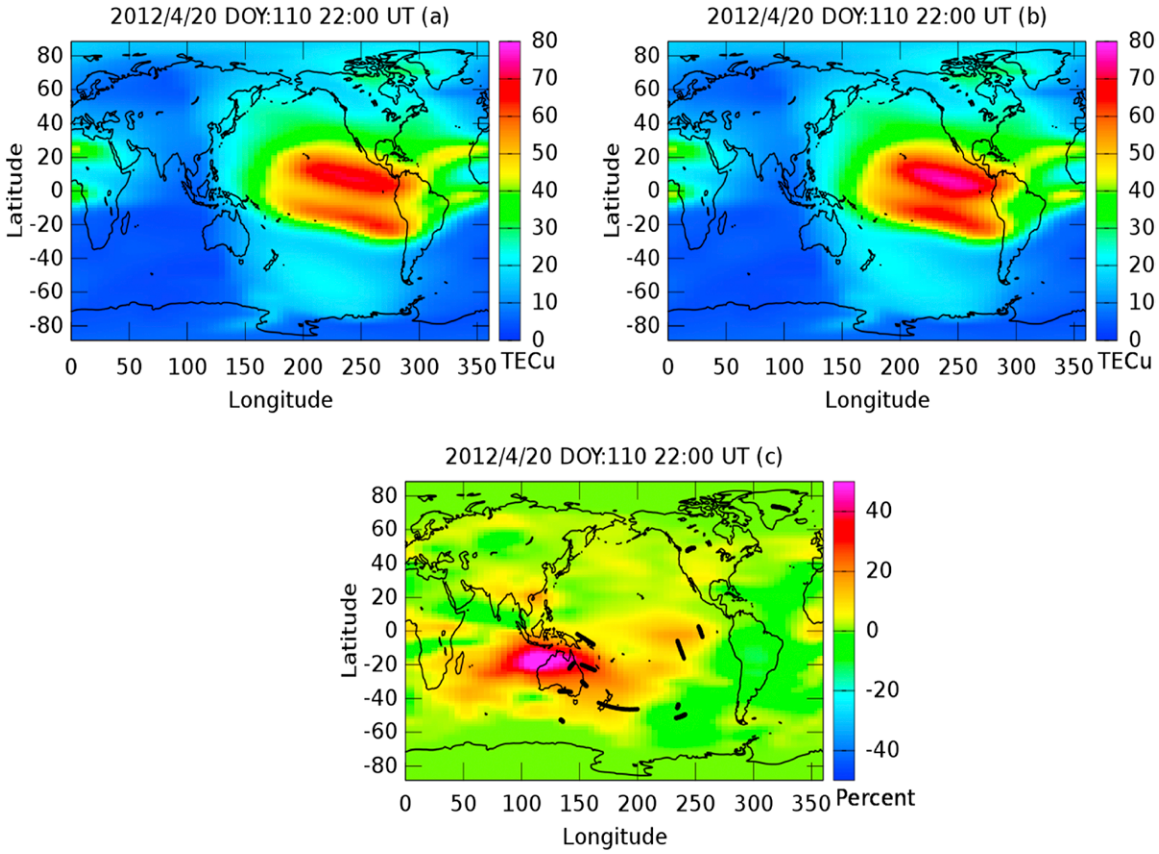


**Fig. 17. Comparison plot for 2200 UT day 110, 2012. (a) TEC from a GAIM data assimilation run without COSMIC occultation data. (b) TEC from a GAIM data assimilation run with COSMIC occultation data. (c) The percent change when adding the COSMIC occultation data (Gardner et al. 2014).**

mass density is critical for satellite drag and orbit prediction. Thus, RO observations have the potential to improve specification of thermosphere density, leading to an improvement in satellite orbit prediction. Lomidze and Scherliess (2015) also combined RO observations and an assimilative technique to infer information about the state of the thermosphere neutral winds. The resulting thermosphere neutral winds were found to be in good agreement with independent ground-based observations.

Yue et al. (2012) reported preliminary results of a global ionosphere electron density reanalysis during 2002–11 based on data assimilation of ground- and space-based TEC observations. The reanalysis used a Kalman filter approach to assimilate the TEC observations into an empirical background model. The reanalysis was found to be in better agreement with independent observations compared to the empirical International Reference Ionosphere (IRI) model, especially after the launch of the six COSMIC satellites in 2006. This study demonstrated the feasibility of generating an upper atmosphere reanalysis. In the future, such reanalysis products may become useful for scientific studies similar to the wide application of atmospheric reanalysis in troposphere–stratosphere research.

## Summary, remaining challenges, and the potential of COSMIC-2

With its high accuracy and precision, high vertical resolution, insensitivity to clouds and precipitation, and global and uniform temporal coverage, COSMIC radio occultation data have had major impacts on weather, climate, and ionospheric science and on numerical weather prediction.

***Some remaining challenges with radio occultation.*** The major challenges for using RO data for weather and climate research and NWP are in the moist tropical lower troposphere and upper stratosphere. In the lower troposphere, the excess phase delay is large, but the amplitude reduces below the noise level due to defocusing and additionally, may undergo strong fluctuations, which impedes accurate measurement of the phase. Negative biases in refractivity in the lower troposphere (below about 3–4 km) may occur due to superrefraction and other factors, especially in the tropics (Sokolovskiy 2003; Ao et al. 2003; Xie et al. 2010b). Positive biases may also occur in the lower troposphere with low SNR due to decrease in the truncation height of the RO signal in the retrieval process because of the asymmetry in the local spectrum of noise in the RO signal (Sokolovskiy et al. 2010b). In addition, we are now at the stage of the science when very detailed studies of all aspects of RO theory and applications, such as a deep analysis of all the terms, as well as the constants, in the complete equation relating refractivity to temperature, water vapor, pressure, and liquid and ice water are useful (e.g., Aparicio et al. 2009; Wee and Kuo 2014; Aparicio and Laroche 2011; Healy 2013). Additional efforts to improve RO retrievals are given by Schreiner (2019). These studies are yielding important fundamental insights into RO and in addition are making small, but cumulatively important enhancements in the accuracy, precision, and utility of RO observations.

Significant issues include uncertainties in bending angle and refractivity retrievals in the lower tropical troposphere and superrefraction in regions dominated sharp planetary boundary layer tops, mainly over oceans. With a sufficiently large SNR (greater than 1,600 V/V), it is possible to identify RO observations affected by superrefraction from the observation itself through the analysis of deep RO signals (signals that propagate below the limb; Sokolovskiy et al. 2014; S. Sokolovskiy 2015, personal communication). This is not possible for current RO observations, but will be possible with the improved COSMIC-2 observations, allowing the use of many more high-quality RO data in the moist lower-troposphere data that are now discarded by simple QC criteria. The error estimates and the presence or not of superrefraction may be used in the subsequent data assimilation process to appropriately weight the observations or discard them altogether.

For the RO retrievals in the upper stratosphere, the main error sources come from ionospheric residual, measurement noise, and initialization of bending angle for Abel retrieval. The impact of large-scale ionospheric residuals on RO retrievals has been modeled previously (Kursinski et al. 1997; Syndergaard 2000; Steiner and Kirchengast 2005; Mannucci et al. 2011) for different local times, different solar activities, and under geomagnetic quiet or disturbed conditions. Residual ionospheric bias can be on the order of 0.1 mrad during daytime solar maximum condition, varying critically with the electron density structure. The bias of RO retrievals under disturbed conditions can be 3 times larger than that in quiet times. In addition, the effect of small-scale ionospheric irregularities (Zeng and Sokolovskiy 2010) can be significant (because they are not eliminated by dual-frequencies ionospheric correction, thus requiring higher-order ionospheric correction methods), but more difficult to estimate. However, recent efforts to correct for the large-scale ionospheric impact appear promising (Angling et al. 2018). The initialization of bending angle can lead to a systematic bias in RO refractivity in the upper levels from the background model or the assumption of isothermal atmosphere. Such systematic biases are difficult to evaluate because the bias of the background model is usually unknown, and can be quite different for different latitudes and seasons. Dynamic determination of the initialization height (widely used in RO centers) based on the relative error covariance between individual RO observation and background model makes the statistical estimation of its impact on RO retrievals even harder. Improving initialization methods is a topic of continuing effort. Recent efforts focus on using bending angle climatologies or averages to improve the background model and reduce the effects of noise (Ao et al. 2012b; Scherllin-Pirscher et al. 2015).

RO electron density profiles are typically retrieved through application of the Abel inversion. While the Abel inversion is a straightforward way to obtain the electron density profile from line-of-sight TEC observations, it assumes the ionosphere is spherically symmetric. This assumption is often invalid, especially in the equatorial region, and can lead to errors as large as 200% in the equatorial region below ~200 km (Yue et al. 2010b). Several approaches have been used to mitigate the error due to the assumption of spherical symmetry. One method is to use a priori knowledge of the horizontal gradients in the inversion (Yue et al. 2013; Pedatella et al. 2015; Tulasi Ram et al. 2016). For example, Pedatella et al. (2015) used monthly mean maps of NmF2 from Abel inverted profiles as a priori information for a subsequent inversion. Wu (2018) minimized the impact of electron density retrieval errors in the D and E region by performing a separate inversion focused on these altitudes. Several alternative approaches have also been proposed (e.g., Schreiner et al. 1999; Hernández-Pajares et al. 2000; Nicolls et al. 2009; Yue et al. 2011), and should also be considered for improving the routine processing of electron density profile retrievals.

***Potential benefits of COSMIC-2.*** Because of the increased SNR, COSMIC-2 will help address the above challenges by providing significant improvements in RO soundings, with reduced biases and more soundings penetrating into the PBL. One of the greatest science opportunities for COSMIC-2 will be in an increased number and quality observations of the tropical and subtropical water vapor distribution, which will support research on the role of water vapor in tropical cyclones and heavy rainfall events, as well as in the global climate system and support improved weather forecasts, especially those of tropical cyclones. Figure 18 shows the average occultation density versus latitude for COSMIC-2 compared to COSMIC-1. The number of occultations in a $500 \times 500$ km$^2$ box over 1 day more than doubles in the tropics for COSMIC-2. However, the elimination of the polar component of COSMIC-2 (https://spacenews.com/u-s-and-taiwan-cancel-second-set-of-cosmic-2-satellites/), which consisted of six satellites in polar orbit, is a significant loss and will be felt in a diminished increase in the impact of RO on forecasting and all the science applications discussed in this paper. This loss may be compensated in part by

other missions, such as described in the Introduction, and commercial providers of RO observations (provided issues related to free and open data access, pricing, and quality can be resolved) (Blum 2019; and these websites: https://spacenews.com/the-still-unrealized-promise-of-commercialearth-science-data/, https://aerospaceamerica.aiaa.org/features/proving-themselves/, www.pbs.org/newshour/show/who-benefits-from-the-privatization-of-weather-data, and https://time.com/5615625/private-companies-weather-forecasting-threat/).

The increased sampling density of COSMIC-2 in the equatorial ionosphere will support advances in ionosphere science and applications, including research into ionospheric variability during geomagnetic storms on shorter time scales. Importantly, COSMIC-2 will provide information pertaining to the altitudinal variability in the ionospheric response to geomagnetic storms, which can give insight into underlying physical drivers of the electron density variations. The improved sampling density of COSMIC-2 will also enable quantitative observational investigations of the short-term variability in the ionosphere due to the lower atmosphere weather, which will help evaluate and improve whole atmosphere–ionosphere models (e.g., H. L. Liu et al. 2018).

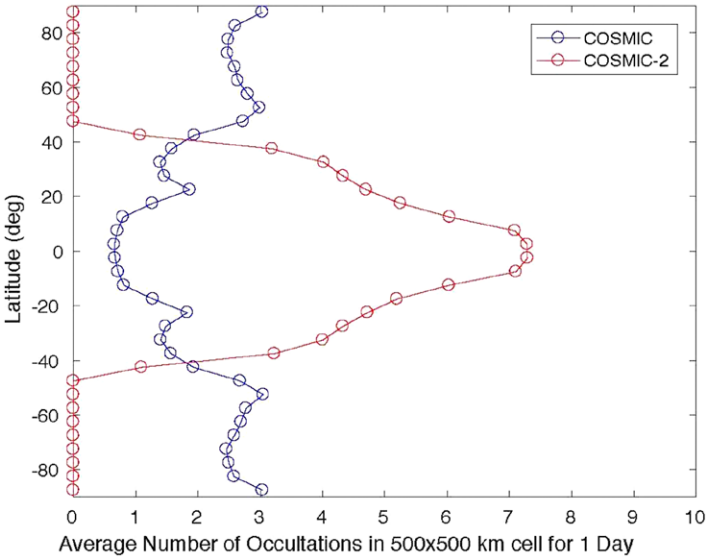


**Fig. 18. The average occultation density vs latitude for COSMIC-2 compared to COSMIC-1 in a 500 × 500 km² box over 1 day.**

Upper-atmosphere data assimilation is a rapidly evolving field. The abundance of COSMIC-2 observations will also provide a critical data source for upper-atmosphere data assimilation models. This will enable improved ionosphere nowcasting and forecasting. Assimilating the RO observations into physics-based models offers the opportunity to gain new insights into thermosphere phenomena, such as the variability in neutral composition, density, and winds.

**Acknowledgments.** We acknowledge the vital support of the late Dr. Jay Fein, of the National Science Foundation (NSF), for his unfailing support of COSMIC, without which COSMIC would not have occurred. Equally important was the support of Drs. C. Y. Tsay and C. H. Liu, as well as the National Science Council and National Space Office in Taiwan. We also thank Eric DeWeaver (NSF) and Jack Kaye and Michael Freilich (NASA) for their critical support over many years. This paper was partially funded by the NSF, NASA, NOAA, and the Copernicus Climate Change Service, which ECMWF implements on behalf of the European Commission. Contributions by A.K.S. were funded by the Austrian Science Fund (FWF) under Project P27724-NBL (VERTICLIM). The National Center for Atmospheric Research is sponsored by the U.S. National Science Foundation. Portions of this research were carried out at the Jet Propulsion Laboratory, California Institute of Technology, under a contract with the National Aeronautics and Space Administration. The manuscript contents are solely the opinions of the author(s) and do not constitute a statement of policy, decision, or position on behalf of NOAA or the U.S. government.

## References


Alexander, S. P., and M. G. Shepherd, 2010: Planetary wave activity in the polar lower stratosphere. *Atmos. Chem. Phys.*, **10**, 707–718, https://doi.org/10.5194/acp-10-707-2010.

——, T. Tsuda, and Y. Kawatani, 2008a: COSMIC GPS observations of Northern Hemisphere winter stratospheric gravity waves and comparisons with an atmospheric general circulation model. *Geophys. Res. Lett.*, **35**, L10808, https://doi.org/10.1029/2008GL033174.

——, ——, ——, and M. Takahashi, 2008b: Global distribution of atmospheric waves in the equatorial upper troposphere and lower stratosphere: COSMIC observations of wave mean flow interactions. *J. Geophys. Res.*, **113**, D24115, https://doi.org/10.1029/2008JD010039.

——, A. R. Klekociuk, M. C. Pitts, A. J. McDonald, and A. Arevalo-Torres, 2011: The effect of orographic gravity waves on Antarctic polar stratospheric cloud occurrence and composition. *J. Geophys. Res.*, **116**, D06109, https://doi.org/10.1029/2010JD015184.

Angling, M. J., S. Elvidge, and S. B. Healy, 2018: Improved model for correcting the ionospheric impact on bending angle in radio occultation measurements. *Atmos. Meas. Tech.*, **11**, 2213–2224, https://doi.org/10.5194/amt-11-2213-2018.

Anthes, R. A., 2011: Exploring Earth's atmosphere with radio occultation: Contributions to weather, climate and space weather. *Atmos. Meas. Tech.*, **4**, 1077–1103, https://doi.org/10.5194/amt-4-1077-2011.

——, and T. Rieckh, 2018: Estimating observation and model error variances using multiple data sets. *Atmos. Meas. Tech.*, **11**, 4239–4260, https://doi.org/10.5194/amt-11-4239-2018.

——, Y.-H. Kuo, D. P. Baumhefner, R. M. Errico, and T. W. Bettge, 1985: Predictability of mesoscale atmospheric motions. *Advances in Geophysics*, Vol. 28, Academic Press, 159–202, https://doi.org/10.1016/S0065-2687(08)60188-0.

——, C. Rocken, and Y.-H. Kuo, 2000: Applications of COSMIC to meteorology and climate. *Terr. Atmos. Oceanic Sci.*, **11**, 115–156, https://doi.org/10.3319/TAO.2000.11.1.115(COSMIC).

——, and Coauthors, 2008: The COSMIC/FORMOSAT-3 mission: Early results. *Bull. Amer. Meteor. Soc.*, **89**, 313–334, https://doi.org/10.1175/BAMS-89-3-313.

Ao, C. O., and A. J. Hajj, 2013: Monitoring the width of the tropical belt with GPS radio occultation measurements. *Geophys. Res. Lett.*, **40**, 6236–6241, https://doi.org/10.1002/2013GL058203.

——, T. K. Meehan, G. A. Hajj, A. J. Mannucci, and G. Beyerle, 2003: Lower troposphere refractivity bias in GPS occultation retrievals. *J. Geophys. Res.*, **108**, 4577, https://doi.org/10.1029/2002JD003216.

——, D. E. Waliser, S. K. Chan, J.-L. Li, B. Tian, F. Xie, and A. J. Mannucci, 2012a: Planetary boundary layer heights from GPS radio occultation refractivity and humidity profiles. *J. Geophys. Res.*, **117**, D16117, https://doi.org/10.1029/2012JD017598.

——, A. J. Mannucci, and E. R. Kursinski, 2012b: Improving GPS Radio occultation stratospheric refractivity retrievals for climate benchmarking. *Geophys. Res. Lett.*, **39**, L12701, https://doi.org/10.1029/2012GL051720.

Aparicio, J. M., and G. Deblonde, 2008: Impact of the assimilation of CHAMP refractivity profiles in Environment Canada global forecasts. *Mon. Wea. Rev.*, **136**, 257–275, https://doi.org/10.1175/2007MWR1951.1.

——, and S. Laroche, 2011: An evaluation of the expression of the atmospheric refractivity for GPS signals. *J. Geophys. Res.*, **116**, D11104, https://doi.org/10.1029/2010JD015214.

——, and ——, 2015: Estimation of the added value of the absolute calibration of GPS radio occultation data for numerical weather prediction. *Mon. Wea. Rev.*, **143**, 1259–1274, https://doi.org/10.1175/MWR-D-14-00153.1.

——, G. Deblonde, L. Garand, and S. Laroche, 2009: Signature of the atmospheric compressibility factor in COSMIC, CHAMP, and GRACE radio occultation data. *J. Geophys. Res.*, **114**, D16114, https://doi.org/10.1029/2008JD011156.

Bauer, P., G. Radnóti, S. Healy, and C. Cardinali, 2014: GNSS radio occultation constellation observing system experiments. *Mon. Wea. Rev.*, **142**, 555–572, https://doi.org/10.1175/MWR-D-13-00130.1.

——, A. Thorpe, and G. Grunet, 2015: The quiet revolution of numerical weather prediction. *Nature*, **525**, 47–55, https://doi.org/10.1038/nature14956.

Biondi, R., T. Neubert, S. Syndergaard, and J. K. Nielsen, 2011: Radio occultation bending angle anomalies during tropical cyclones. *Atmos. Meas. Tech.*, **4**, 1053–1060, https://doi.org/10.5194/amt-4-1053-2011.

——, W. J. Randel, S.-P. Ho, T. Neubert, and S. Syndergaard, 2012: Thermal structure of intense convective clouds derived from GPS radio occultations. *Atmos. Chem. Phys.*, **12**, 5309–5318, https://doi.org/10.5194/acp-12-5309-2012.

——, S.-P. Ho, W. J. Randel, T. Neubert, and S. Syndergaard, 2013: Tropical cyclone cloud-top height and vertical temperature structure detection using GPS radio occultation measurements. *J. Geophys. Res. Atmos.*, **118**, 5247–5259, https://doi.org/10.1002/jgrd.50448.

——, A. K. Steiner, G. Kirchengast, and T. Rieckh, 2015: Characterization of thermal structure and conditions for overshooting of tropical and extratropical cyclones with GPS radio occultation. *Atmos. Chem. Phys.*, **15**, 5181–5193, https://doi.org/10.5194/acp-15-5181-2015.

Birner, T., 2010: Recent widening of the tropical belt from global tropopause statistics: Sensitivities. *J. Geophys. Res.*, **115**, D23109, https://doi.org/10.1029/2010JD014664.

Blum, A., 2019: *The Weather Machine: How We See into the Future*. Vintage, 224 pp.

Bonafoni, S., R. Biondi, H. Brenot, and R. Anthes, 2019: Radio occultation and ground-based GNSS products for observing, understanding and predicting extreme events: A review. *Atmos. Res.*, **230**, 104624, https://doi.org/10.1016/j.atmosres.2019.104624.

Bonavita, M., 2014: On some aspects of the impact of GPSRO observations in global numerical weather prediction. *Quart. J. Roy. Meteor. Soc.*, **140**, 2546–2562, https://doi.org/10.1002/qj.2320.

Brahmanandam, P. S., Y. H. Chu, and J. Liu, 2010: Observations of equatorial Kelvin wave modes in the FORMOSAT-3/COSMIC GPS RO temperature profiles. *Terr. Atmos. Ocean. Sci.*, **21**, 829–840, https://doi.org/10.3319/TAO.2010.01.06.01(A).

Brewer, A. W., 1949: Evidence for a world circulation provided by the measurements of helium and water vapour distribution in the stratosphere. *Quart. J. Roy. Meteor. Soc.*, **75**, 351–363, https://doi.org/10.1002/qj.49707532603.

Brunner, L., and A. K. Steiner, 2017: A global perspective on atmospheric blocking using GPS radio occultation—One decade of observations. *Atmos. Meas. Tech.*, **10**, 4727–4745, https://doi.org/10.5194/amt-10-4727-2017.

——, ——, B. Scherllin-Pirscher, and M. W. Jury, 2016: Exploring atmospheric blocking with GPS radio occultation observations. *Atmos. Chem. Phys.*, **16**, 4593–4604, https://doi.org/10.5194/acp-16-4593-2016.

Cardinali, C., 2009: Monitoring the observation impact on the short-range forecast. *Quart. J. Roy. Meteor. Soc.*, **135**, 239–250, https://doi.org/10.1002/qj.366.

——, and S. Healy, 2014: Impact of GPS radio occultation measurements in the ECMWF system using adjoint-based diagnostics. *Quart. J. Roy. Meteor. Soc.*, **140**, 2315–2320, https://doi.org/10.1002/qj.2300.

Carter, B. A., K. Zhang, R. Norman, V. V. Kumar, and S. Kumar, 2013: On the occurrence of equatorial F-region irregularities during solar minimum using radio occultation measurements. *J. Geophys. Res. Space Phys.*, **118**, 892–904, https://doi.org/10.1002/jgra.50089.

Chau, J. L., L. P. Goncharenko, B. G. Fejer, and H.-L. Liu, 2012: Equatorial and low latitude ionospheric effects during sudden stratospheric warming events. *Space Sci. Rev.*, **168**, 385–417, https://doi.org/10.1007/s11214-011-9797-5.

Chen, S.-Y., T.-K. Wee, Y. H. Kuo, and D. H. Bromwich, 2014: An impact assessment of GPS radio occultation data on prediction of a rapidly developing cyclone over the Southern Ocean. *Mon. Wea. Rev.*, **142**, 4187–4206, https://doi.org/10.1175/MWR-D-14-00024.1.

Chen, X. M., and Coauthors, 2018: The impact of radio occultation observations on the simulation of Hurricane Karl (2010). *Mon. Wea. Rev.*, **146**, 329–350, https://doi.org/10.1175/MWR-D-17-0001.1.

Chen, Y. C., M. E. Hsieh, L. F. Hsiao, Y.-H. Kuo, M. J. Yang, C.-Y. Huang, and C. S. Lee, 2015: Systematic evaluation of the impacts of GPSRO data on the prediction of typhoons over the northwestern Pacific in 2008–2010. *Atmos. Meas. Tech.*, **8**, 2531–2542, https://doi.org/10.5194/amt-8-2531-2015.

Collard, A., and S. B. Healy, 2003: The combined impact of future space-based atmospheric sounding instruments on numerical weather prediction analysis

fields: A simulation study. *Quart. J. Roy. Meteor. Soc.*, **129**, 2741–2760, https://doi.org/10.1256/qj.02.124.

Cucurull, L., 2010: Improvement in the use of an operational constellation of GPS radio occultation receivers in weather forecasting. *Wea. Forecasting*, **25**, 749–767, https://doi.org/10.1175/2009WAF2222302.1.

——, J. C. Derber, and R. J. Purser, 2013: A bending angle forward operator for global positioning system radio occultation measurements. *J. Geophys. Res. Atmos.*, **118**, 14–28, https://doi.org/10.1029/2012JD017782.

——, R. A. Anthes, and L.-L. Tsao, 2014: Radio occultation observations as anchor observations in numerical weather prediction models and associated reduction of bias corrections in microwave and infrared satellite observations. *J. Atmos. Oceanic Technol.*, **31**, 20–32, https://doi.org/10.1175/JTECH-D-13-00059.1.

Davis, N. A., and T. Birner, 2013: Seasonal to multidecadal variability of the width of the tropical belt. *J. Geophys. Res. Atmos.*, **118**, 7773–7787, https://doi.org/10.1002/jgrd.50610.

Davis, S. M., and Coauthors, 2017: Assessment of upper tropospheric and stratospheric water vapor and ozone in reanalyses as part of S-RIP. *Atmos. Chem. Phys.*, **17**, 12 743–12 778, https://doi.org/10.5194/acp-17-12743-2017.

Dee, D. P., 2005: Bias and data assimilation. *Quart. J. Roy. Meteor. Soc.*, **131**, 3323–3343, https://doi.org/10.1256/qj.05.137.

——, and Coauthors, 2011: The ERA-Interim reanalysis: Configuration and performance of the data assimilation system. *Quart. J. Roy. Meteor. Soc.*, **137**, 553–597, https://doi.org/10.1002/qj.828.

Desroziers, G., L. Berre, B. Chapnik, and P. Poli, 2005: Diagnosis of observation, background and analysis-error statistics in observation space. *Quart. J. Roy. Meteor. Soc.*, **131**, 3385–3396, https://doi.org/10.1256/qj.05.108.

Eyre, J. R., 1994: Assimilation of radio occultation measurements into a numerical weather prediction system. ECMWF Tech. Memo. 199, 34 pp., www.ecmwf.int/node/9331.

——, 2016: Observation bias correction schemes in data assimilation systems: A theoretical study of some of their properties. *Quart. J. Roy. Meteor. Soc.*, **142**, 2284–2291, https://doi.org/10.1002/qj.2819.

Faber, A., P. Llamedo, T. Schmidt, A. de la Torre, and J. Wickert, 2013: On the determination of gravity wave momentum flux from GPS radio occultation data. *Atmos. Meas. Tech.*, **6**, 3169–3180, https://doi.org/10.5194/amt-6-3169-2013.

Fetzer, E. J., B. H. Lambrigtsen, A. Eldering, H. H. Aumann, and M. T. Chahine, 2006: Biases in total precipitable water vapor climatologies from Atmospheric Infrared Sounder and Advanced Microwave Scanning Radiometer. *J. Geophys. Res.*, **111**, D09S16, https://doi.org/10.1029/2005JD006598.

——, and Coauthors, 2008: Comparison of upper tropospheric water vapor observations from the Microwave Limb Sounder and Atmospheric Infrared Sounder. *J. Geophys. Res.*, **113**, D22110, https://doi.org/10.1029/2008JD010000.

Flannaghan, T. J., and S. Fueglistaler, 2013: The importance of the tropical tropopause layer for equatorial Kelvin wave propagation. *J. Geophys. Res. Atmos.*, **118**, 5160–5175, https://doi.org/10.1002/jgrd.50418.

Foelsche, U., B. Pirscher, M. Borsche, G. Kirchengast, and J. Wickert, 2009: Assessing the climate monitoring utility of radio occultation data: From CHAMP to FORMOSAT-3/COSMIC. *Terr. Atmos. Ocean. Sci.*, **20**, 155–170, https://doi.org/10.3319/TAO.2008.01.14.01(F3C).

Gardner, L. C., R. W. Schunk, L. Scherliess, J. J. Sojka, and L. Zhu, 2014: Global assimilation of ionospheric measurements-Gauss Markov model: Improved specifications with multiple data types. *Space Wea.*, **12**, 675–688, https://doi.org/10.1002/2014SW001104.

Geer, A. J., and Coauthors, 2017: The growing impact of satellite observations sensitive to humidity, cloud and precipitation. *Quart. J. Roy. Meteor. Soc.*, **143**, 3189–3206, https://doi.org/10.1002/qj.3172.

Gelaro, R., and Coauthors, 2017: The Modern-Era Retrospective Analysis for Research and Applications, version 2 (MERRA-2). *J. Climate*, **30**, 5419–5454, https://doi.org/10.1175/JCLI-D-16-0758.1.

Gilpin, S., R. Anthes, and S. Sokolovskiy, 2019: Sensitivity of forward-modeled bending angles to vertical interpolation of refractivity for radio occultation data assimilation. *Mon. Wea. Rev.*, **147**, 269–289, https://doi.org/10.1175/MWR-D-18-0223.1.

Goody, R., J. Anderson, and G. North, 1998: Testing climate models: An approach. *Bull. Amer. Meteor. Soc.*, **79**, 2541–2549, https://doi.org/10.1175/1520-0477(1998)079<2541:TCMAA>2.0.CO;2.

Grise, K. M., D. W. J. Thompson, and T. Birner, 2010: A global survey of static stability in the stratosphere and upper troposphere. *J. Climate*, **23**, 2275–2292, https://doi.org/10.1175/2009JCLI3369.1.

Guo, P., Y.-H. Kuo, S. V. Sokolovskiy, and D. H. Lenschow, 2011: Estimating atmospheric boundary layer depth using COSMIC radio occultation data. *J. Atmos. Sci.*, **68**, 1703–1713, https://doi.org/10.1175/2011JAS3612.1.

Haase, J. S., B. J. Murphy, P. Muradyan, F. Nievinski, K. M. Larson, J. L. Garrison, and K.-N. Wang, 2014: First results from an airborne GPS radio occultation system for atmospheric profiling. *Geophys. Res. Lett*, **41**, 1759–1765, https://doi.org/10.1002/2013GL058681.

Hajj, G. A., and Coauthors, 2004: CHAMP and SAC-C atmospheric occultation results and intercomparisons. *J. Geophys. Res.*, **109**, D06109, https://doi.org/10.1029/2003JD003909.

He, W., S.-P. Ho, H. Chen, X. Zhou, D. Hunt, and Y. Kuo, 2009: Assessment of radiosonde temperature measurements in the upper troposphere and lower stratosphere using COSMIC radio occultation data. *Geophys. Res. Lett.*, **36**, L17807, https://doi.org/10.1029/2009GL038712.

Healy, S. B., 2008: Forecast impact experiment with a constellation of GPS radio occultation receivers. *Atmos. Sci. Lett.*, **9**, 111–118, https://doi.org/10.1002/asl.169.

——, 2013: Surface pressure information retrieved from GPS radio occultation measurements. *Quart. J. Roy. Meteor. Soc.*, **139**, 2108–2118, https://doi.org/10.1002/qj.2090.

——, 2014: Implementation of the ROPP two-dimensional bending angle observation operator in an NWP system. EUMETSAT Radio Occultation Meteorology Satellite Application Facility Rep. 19, 33 pp., www.romsaf.org/general-documents/rsr/rsr_19.pdf.

——, and J. Thépaut, 2006: Assimilation experiments with CHAMP GPS radio occultation measurements. *Quart. J. Roy. Meteor. Soc.*, **132**, 605–623, https://doi.org/10.1256/qj.04.182.

——, A. M. Jupp, and C. Marquardt, 2005: Forecast impact experiment with GPS radio occultation measurements. *Geophys. Res. Lett.*, **32**, L03804, https://doi.org/10.1029/2004GL020806.

——, J. R. Eyre, M. Hamrun, and J. N. Thépaut, 2007: Assimilating GPS radio occultation measurements with two-dimensional bending angle observation operators. *Quart. J. Roy. Meteor. Soc.*, **133**, 1213–1227, https://doi.org/10.1002/qj.63.

Hernández-Pajares, M., J. M. Juan, and J. Sanz, 2000: Improving the Abel inversion by adding ground GPS data to LEO radio occultations in ionospheric sounding. *Geophys. Res. Lett.*, **27**, 2473–2476, https://doi.org/10.1029/2000GL000032.

Hersbach, H., and D. Dee, 2016: ERA5 reanalysis is in production. *ECMWF Newsletter*, No. 147, ECMWF, Reading, United Kingdom, 7, www.ecmwf.int/sites/default/files/elibrary/2016/16299-newsletter-no147-spring-2016.pdf.

——, and Coauthors, 2018: Operational global reanalysis: Progress, future directions and synergies with NWP. ECMWF ERA Rep. 27, 63 pp., www.ecmwf.int/en/elibrary/18765-operational-global-reanalysis-progress-future-directions-and-synergies-nwp.

Hindley, N. P., C. J. Wright, N. D. Smith, and N. J. Mitchell, 2015: The southern stratospheric gravity wave hot spot: Individual waves and their momentum fluxes measured by COSMIC GPS-RO. *Atmos. Chem. Phys.*, **15**, 7797–7818, https://doi.org/10.5194/acp-15-7797-2015.

Ho, S.-P., Y. H. Kuo, Z. Zeng, and T. C. Peterson, 2007: A comparison of lower stratosphere temperature from microwave measurements with CHAMP GPS RO data. *Geophys. Res. Lett.*, **34**, L15701, https://doi.org/10.1029/2007GL030202.

——, M. Goldberg, Y.-H. Kuo, C.-Z. Zou, and W. Schreiner, 2009a: Calibration of temperature in the lower stratosphere from microwave measurements using COSMIC radio occultation data: Preliminary results. *Terr. Atmos. Ocean. Sci.*, **20**, 87, https://doi.org/10.3319/TAO.2007.12.06.01(F3C).

——, and Coauthors, 2009b: Estimating the uncertainty of using GPS radio occultation data for climate monitoring: Intercomparison of CHAMP refractivity climate records from 2002 to 2006 from different data centers. *J. Geophys. Res.*, **114**, D23107, https://doi.org/10.1029/2009JD011969.

——, Y.-H. Kuo, W. Schreiner, and X. Zho, 2010a: Using SI-traceable global positioning system radio occultation measurements for climate monitoring [in "State of the Climate in 2009"]. *Bull. Amer. Meteor. Soc.*, **91** (7), S36–S37, https://doi.org/10.1175/BAMS-91-7-StateoftheClimate.

——, X. Zhou, Y.-H. Kuo, D. Hunt, and J.-H. Wang, 2010b: Global evaluation of radiosonde water vapor systematic biases using GPS radio occultation from COSMIC and ECMWF analysis. *Remote Sens.*, **2**, 1320–1330, https://doi.org/10.3390/rs2051320.

——, and Coauthors, 2012: Reproducibility of GPS radio occultation data for climate monitoring: Profile-to-profile inter-comparison of CHAMP climate records 2002 to 2008 from six data centers. *J. Geophys. Res.*, **117**, D18111, https://doi.org/10.1029/2012JD017665.

——, X. Yue, Z. Zeng, C. Ao, C.-Y. Huang, E. R. Kursinski, and Y.-H. Kuo, 2014: Applications of COSMIC radio occultation data from the troposphere to ionosphere and potential impacts of COSMIC-2 data. *Bull. Amer. Meteor. Soc.*, **95**, ES18–ES22, https://doi.org/10.1175/BAMS-D-13-00035.1.

——, L. Peng, R. A. Anthes, Y.-H. Kuo, and H.-C. Lin 2015: Marine boundary layer heights and their longitudinal, diurnal, and interseasonal variability in the southeastern Pacific using COSMIC, CALIOP, and radiosonde data. *J. Climate*, **28**, 2856–2872, https://doi.org/10.1175/JCLI-D-14-00238.1.

——, ——, and H. Voemel, 2017: Characterization of the long-term radiosonde temperature biases in the upper troposphere and lower stratosphere using COSMIC and MetOp-A/GRAS data from 2006 to 2014. *Atmos. Chem. Phys.*, **17**, 4493–4511, https://doi.org/10.5194/acp-17-4493-2017.

——, ——, C. Mears, and R. Anthes, 2018: Comparison of global observations and trends of total precipitable water derived from microwave radiometers and COSMIC radio occultation from 2006 to 2013. *Atmos. Chem. Phys.*, **18**, 259–274, https://doi.org/10.5194/acp-18-259-2018.

——, R. A. Anthes, H. Zhang, S. Chen, 2019: Improving the impact of radio occultation observations on numerical forecasts of tropical cyclones. *JCSDA Quarterly Newsletter*, No. 62, Joint Center for Satellite Data Assimilation, Boulder, CO, 11–17.

Huang, C.-Y., Y.-H. Kuo, and S.-H. Chen, 2005: Improvements on typhoon forecast with assimilated GPS occultation refractivity. *Wea. Forecasting*, **20**, 931–953, https://doi.org/10.1175/WAF874.1.

——, W.-H. Teng, S.-P. Ho, and Y. H. Kuo, 2013: Global variation of COSMIC precipitable water over land: Comparisons with ground-based GPS measurements and NCEP reanalyses. *Geophys. Res. Lett.*, **40**, 5327–5331, https://doi.org/10.1002/GRL.50885.

Jin, H., and Coauthors, 2011: Vertical connection from the tropospheric activities to the ionospheric longitudinal structure simulated by a new Earth's whole atmosphere-ionosphere coupled model. *J. Geophys. Res.*, **116**, A01316, https://doi.org/10.1029/2010JA015925.

——, Y. Miyoshi, D. Pancheva, P. Mukhtarov, H. Fujiwara, and H. Shinagawa, 2012: Response of migrating tides to the stratospheric sudden warming in 2009 and their effects on the ionosphere studied by a whole atmosphere-ionosphere model GAIA with COSMIC and TIMED/SABER observations. *J. Geophys. Res.*, **117**, A10323, https://doi.org/10.1029/2012JA017650.

John, V. O., and B. J. Soden, 2007: Temperature and humidity biases in global climate models and their impact on climate feedbacks. *Geophys. Res. Lett.*, **34**, L18704, https://doi.org/10.1029/2007GL030429.

Khaykin, S. M., A. Hauchecorne, N. Mzé, and P. Keckhut, 2015: Seasonal variation of gravity wave activity at midlatitudes from 7 years of COSMIC GPS and Rayleigh lidar temperature observations. *Geophys. Res. Lett.*, **42**, 1251–1258, https://doi.org/10.1002/2014GL062891.

Kim, J., and S.-W. Son, 2012: Tropical cold-point tropopause: Climatology, seasonal cycle, and intraseasonal variability derived from COSMIC GPS radio occultation measurements. *J. Climate*, **25**, 5343–5360, https://doi.org/10.1175/JCLI-D-11-00554.1.

——, W. J. Randel, and T. Birner, 2018: Convectively driven tropopause-level cooling and its influences on stratospheric moisture. *J. Geophys. Res. Atmos.*, **123,** 590–606, https://doi.org/10.1002/2017JD027080.

Kim, J. E., and M. J. Alexander, 2015: Direct impacts of waves on tropical cold point tropopause temperature. *Geophys. Res. Lett.*, **42**, 1584–1592, https://doi.org/10.1002/2014GL062737.

Kobayashi, S., and Coauthors, 2015: The JRA-55 Reanalysis: General specifications and basic characteristics. *J. Meteor. Soc. Japan*, **93**, 5–48, https://doi.org/10.2151/jmsj.2015-001.

Kueh, M.-T., C.-Y. Huang, S.-Y. Chen, S.-H. Chen, and C.-J. Wang, 2009: Impact of GPS radio occultation refractivity soundings on a simulation of Typhoon Bilis (2006) upon landfall. *Terr. Atmos. Ocean. Sci.*, **20**, 115–131, https://doi.org/10.3319/TAO.2008.01.21.03(F3C).

Kuo, Y.-H., T.-K. Wee, S. Sokolovskiy, C. Rocken, W. Schreiner, D. Hunt, and R. A. Anthes, 2004: Inversion and error estimation of GPS radio occultation data. *J. Meteor. Soc. Japan*, **82**, 507–531, https://doi.org/10.2151/jmsj.2004.507.

——, H. Liu, Y.-R. Guo, C.-T. Terng, and Y.-T. Lin, 2009: Impact of FORMOSAT-3/COSMIC data on typhoon and mei-yu prediction. *Recent Progress in Atmospheric Sciences: Applications to the Asia-Pacific Region*, K.-N. Liou and M. D. Chou, Eds., World Scientific, 458–483.

——, S. Y. Chen, and T. J. Galarneau Jr., 2016: Impact of GPS radio occultation data on the prediction of tropical cyclogenesis. *30th Conf. on Hydrology*, New Orleans, LA, Amer. Meteor. Soc., J19.1, https://ams.confex.com/ams/96Annual/webprogram/Paper277532.html.

Kursinski, E. R., and T. Gebhardt, 2014: A method to deconvolve errors in GPS RO-derived water vapor histograms. *J. Atmos. Oceanic Technol.*, **31**, 2606–2628, https://doi.org/10.1175/JTECH-D-13-00233.1.

——, G. A. Hajj, J. T. Schofield, R. P. Linfield, and K. R. Hardy, 1997: Observing Earth's atmosphere with radio occultation measurements using the global positioning system. *J. Geophys. Res.*, **102**, 23 429–23 465, https://doi.org/10.1029/97JD01569.

——, ——, S. S. Leroy, and B. Herman, 2000: The GPS radio occultation technique. *Terr. Atmos. Ocean. Sci.*, **11**, 53–114, https://doi.org/10.3319/TAO.2000.11.1.53(COSMIC).

Lackner, B. C., A. K. Steiner, G. Kirchengast, and G. C. Hegerl, 2011: Atmospheric climate change detection by radio occultation data using a fingerprinting method. *J. Climate*, **24**, 5275–5291, https://doi.org/10.1175/2011JCLI3966.1.

Ladstädter, F., A. K. Steiner, U. Foelsche, L. Haimberger, C. Tavolato, and G. Kirchengast, 2011: An assessment of differences in lower stratospheric temperature records from (A)MSU, radiosondes, and GPS radio occultation. *Atmos. Meas. Tech.*, **4**, 1965–1977, https://doi.org/10.5194/amt-4-1965-2011.

——, ——, M. Schwärz, and G. Kirchengast, 2015: Climate intercomparison of GPS radio occultation, RS90/92 radiosondes and GRUAN from 2002 to 2013. *Atmos. Meas. Tech.*, **8**, 1819–1834, https://doi.org/10.5194/amt-8-1819-2015.

Lee, I. T., W. Wang, J. Y. Liu, C. Y. Chen, and C. H. Lin, 2011: The ionospheric midlatitude trough observed by FORMOSAT-3/COSMIC during solar minimum. *J. Geophys. Res.*, **116**, A06311, https://doi.org/10.1029/2010JA015544.

Lewis, H. W., 2009: A robust method for tropopause altitude identification using GPS radio occultation data. *Geophys. Res. Lett.*, **36**, L12808, https://doi.org/10.1029/2009GL039231.

Lin, C. H., J. T. Lin, L. C. Chang, J. Y. Liu, C. H. Chen, W. H. Chen, H. H. Huang, and C. H. Liu, 2012: Observation of global ionospheric responses to the 2009 stratosphere sudden warming event by FORMOSAT-3/COSMIC. *J. Geophys. Res.*, **117**, A06323, https://doi.org/10.1029/2011JA017230.

——, ——, ——, W. H. Chen, C. H. Chen, and J. Y. Liu, 2013: Stratospheric sudden warming effects on the ionospheric migrating tides during 2008–2010 observed by FORMOSAT-3/COSMIC. *J. Atmos. Sol.-Terr. Phys.*, **103**, 66–75, https://doi.org/10.1016/j.jastp.2013.03.026.

Lin, C. Y., T. Matsuo, J. Y. Liu, C. H. Lin, H. F. Tsai, and E. A. Araujo-Pradere, 2015: Ionospheric assimilation of radio occultation and ground-based GPS data using non-stationary background model error covariance. *Atmos. Meas. Tech.*, **8**, 171–182, https://doi.org/10.5194/amt-8-171-2015.

Lin, J. T., C. H. Lin, L. C. Chang, H. H. Huang, J. Y. Liu, A. B. Chen, C. H. Chen, and C. H. Liu, 2012: Observational evidence of ionospheric migrating tide modification during the 2009 stratospheric sudden warming. *Geophys. Res. Lett.*, **39**, L02101, https://doi.org/10.1029/2011GL050248.

Liu, H., J. Anderson, and Y.-H. Kuo, 2012: Improved analyses and forecasts of Hurricane Ernesto's genesis using radio occultation data in an ensemble filter

assimilation system. *Mon. Wea. Rev.*, **140**, 151–166, https://doi.org/10.1175/MWR-D-11-00024.1.

——, Y.-H. Kuo, S. Sokolovskiy, X. Zou, Z. Zeng, L.-F. Hsiao, and B.C. Ruston, 2018: A quality control procedure based on bending angle measurement uncertainty for radio occultation data assimilation in the tropical lower troposphere. *J. Atmos. Oceanic Technol.*, **35**, 2117–2131, https://doi.org/10.1175/JTECH-D-17-0224.1.

Liu, H. L., and Coauthors, 2018: Development and validation of the Whole Atmosphere Community Climate Model with thermosphere and ionosphere extension (WACCM-X2.0). *J. Adv. Model. Earth Syst.*, **10**, 381–402, https://doi.org/10.1002/2017MS001232.

Lomidze, L., and L. Scherliess, 2015: Estimation of thermospheric zonal and meridional winds using a Kalman filter technique. *Space Wea.*, **13**, 747–760, https://doi.org/10.1002/2015SW001250.

Long, C. S., M. Fujiwara, S. Davis, D. M. Mitchell, and C. J. Wright, 2017: Climatology and interannual variability of dynamic variables in multiple reanalyses evaluated by the SPARC Reanalysis Intercomparison Project (S-RIP). *Atmos. Chem. Phys.*, **17**, 14 593–14 629, https://doi.org/10.5194/acp-17-14593-2017.

Luna, D., P. Alexander, and A. de la Torre, 2013: Evaluation of uncertainty in gravity wave potential energy calculations through GPS radio occultation measurements. *Adv. Space Res.*, **52**, 879–882, https://doi.org/10.1016/j.asr.2013.05.015.

Ma, Z., Y.-H. Kuo, B. Wang, W.-S. Wu, and S. Sokolovskiy, 2009: Comparison of local and nonlocal observation operators for the assimilation of GPS RO data with the NCEP GSI system: An OSSE study. *Mon. Wea. Rev.*, **137**, 3575–3587, https://doi.org/10.1175/2009MWR2809.1.

Mannucci, A. J., C. O. Ao, X. Pi, and B. A. Iijima, 2011: The impact of large scale ionospheric structure on radio occultation retrievals. *Atmos. Meas. Tech.*, **4**, 2837–2850, https://doi.org/10.5194/amt-4-2837-2011.

Matsuo, T., I.-T. Lee, and J. L. Anderson, 2013: Thermospheric mass density specification using an ensemble Kalman filter. *J. Geophys. Res. Space Phys.*, **118**, 1339–1350, https://doi.org/10.1002/jgra.50162.

McDonald, A. J., 2012: Gravity wave occurrence statistics derived from paired COSMIC/FORMOSAT3 observations. *J. Geophys. Res.*, **117**, D15106, https://doi.org/10.1029/2011JD016715.

McNally, A. P., P. D. Watts, J. A. Smith, R. Engelen, G. A. Kelly, J. N. Thépaut, and M. Matricardi, 2006: The assimilation of AIRS radiance data at ECMWF. *Quart. J. Roy. Meteor. Soc.*, **132**, 935–957, https://doi.org/10.1256/qj.04.171.

Mears, C., S. P. Ho, J. Wang, H. Huelsing, and L. Peng, 2017: Total column water vapor [in "States of the Climate in 2016"]. *Bull. Amer. Meteor. Soc.*, **98** (8), S24–S25, https://doi.org/10.1175/2017BAMSStateoftheClimate.1.

Melbourne, W. G., and Coauthors, 1994: The application of spaceborne GPS to atmospheric limb sounding and global change monitoring, JPL Publ. 94–18, NASA Jet Propulsion Laboratory, Pasadena, CA, 147 pp., https://ntrs.nasa.gov/archive/nasa/casi.ntrs.nasa.gov/19960008694.pdf.

Ming, F. C., C. Ibrahim, C. Barthe, S. Jolivet, P. Keckhut, Y. A. Liou, and Y. Kuleshov, 2014: Observations and a numerical study of gravity waves during tropical cyclone Ivan (2008). *Atmos. Chem. Phys.*, **14**, 641–658, https://doi.org/10.5194/acp-14-641-2014.

Murphy, B. J., J. S. Haase, P. Muradyan, J. L. Garrison, and K.-N. Wang, 2015: Airborne GPS radio occultation refractivity profiles observed in tropical storm environments. *J. Geophys. Res. Atmos.*, **120**, 1690–1709, https://doi.org/10.1002/2014JD022931.

Nash, J., T. Oakley, H. Vömel, and L. Wei, 2011: WMO intercomparison of high quality radiosonde systems. Instruments and Observing Methods Rep. 107, 238 pp., WMO/TD-1580.

Nath, D., W. Chen, and A. Guharay, 2015: Climatology of stratospheric gravity waves and their interaction with zonal mean wind over the tropics using GPS RO and ground-based measurements in the two phases of QBO. *Theor. Appl. Climatol.*, **119**, 757–769, https://doi.org/10.1007/s00704-014-1146-7.

Neiman, P. J., F. M. Ralph, G. A. Wick, Y.-H. Kuo, T.-K. Wee, Z. Ma, G. H. Taylor, and M. D. Dettinger, 2008:Diagnosis of an intense atmospheric river impacting the Pacific Northwest: Storm summary and offshore vertical structure observed with COSMIC satellite retrieval. *Mon. Wea. Rev.*, **136**, 4398–4420, https://doi.org/10.1175/2008MWR2550.1.

Nicolls, M. J., F. S. Rodrigues, G. S. Bust, and J. L. Chau, 2009: Estimating E region density profiles from radio occultation measurements assisted by IDA4D. *J. Geophys. Res.*, **114**, A10316, https://doi.org/10.1029/2009JA014399.

Noël, S., M. Buchwitz, and J. P. Burrows, 2004: First retrieval of global water vapour column amounts from SCIAMACHY measurements. *Atmos. Chem. Phys.*, **4**, 111–125, https://doi.org/10.5194/acp-4-111-2004.

Ohring, G., Ed., 2007: Achieving Satellite Instrument Calibration for Climate Change (ASIC3). Workshop Rep., NOAA, Camp Springs, MD, 144 pp., www.star.nesdis.noaa.gov/star/documents/ASIC3-071218-webversfinal.pdf.

Oyama, K.-I., J. T. Jhou, J. T. Lin, C. Lin, H. Liu, and K. Yumoto, 2014: Ionospheric response to 2009 sudden stratospheric warming in the Northern Hemisphere. *J. Geophys. Res. Space Phys.*, **119**, 10 260–10 275, https://doi.org/10.1002/2014JA020014.

Pan, C. J., U. Das, S. S. Yang, C. J. Wong, and H. C. Lai, 2011: Investigation of Kelvin waves in the stratosphere using FORMOSAT-3/COSMIC temperature data. *J. Meteor. Soc. Japan*, **89A**, 83–96, https://doi.org/10.2151/jmsj.2011-A05.

Pedatella, N. M., and A. Maute, 2015: Impact of the semidiurnal lunar tide on the midlatitude thermospheric wind and ionosphere during sudden stratosphere warmings. *J. Geophys. Res. Space Phys.*, **120**, 10 740–10 753, https://doi.org/10.1002/2015JA021986.

——, H.-L. Liu, F. Sassi, J. Lei, J. L. Chau, and X. Zhang, 2014: Ionosphere variability during the 2009 SSW: Influence of the lunar semidiurnal tide and mechanisms producing electron density variability. *J. Geophys. Res. Space Phys.*, **119**, 3828–3843, https://doi.org/10.1002/2014JA019849.

——, X. Yue, and W. S. Schreiner, 2015: An improved inversion for FORMOSAT-3/COSMIC ionosphere electron density profiles. *J. Geophys. Res. Space Phys.*, **120**, 8942–8953, https://doi.org/10.1002/2015JA021704.

Pirscher, B., U. Foelsche, M. Borsche, G. Kirchengast, and Y.-H. Kuo, 2010: Analysis of migrating diurnal tides detected in FORMOSAT-3/COSMIC temperature data. *J. Geophys. Res.*, **115**, D14108, https://doi.org/10.1029/2009JD013008.

Poli, P., P. Moll, D. Puech, F. Rabier, and S. B. Healy, 2009: Quality control, error analysis, and impact assessment of FORMOSAT-3/COSMIC in numerical weather prediction. *Terr. Atmos. Ocean. Sci.*, **20**, 101–113, https://doi.org/10.3319/TAO.2008.01.21.02(F3C).

——, S. B. Healy, and D. P. Dee, 2010: Assimilation of global positioning system radio occultation data in the ECMWF ERA-Interim reanalysis. *Quart. J. Roy. Meteor. Soc.*, **136**, 1972–1990, https://doi.org/10.1002/qj.722.

Randel, W. J., and F. Wu, 2005: Kelvin wave variability near the equatorial tropopause observed in GPS radio occultation measurements. *J. Geophys. Res.*, **110**, D03102, https://doi.org/10.1029/2004JD005006.

——, and ——, 2010: The polar summer tropopause inversion layer. *J. Atmos. Sci.*, **67**, 2572–2581, https://doi.org/10.1175/2010JAS3430.1.

——, and ——, 2015: Variability of zonal mean tropical temperatures derived from a decade of GPS radio occultation data. *J. Atmos. Sci.*, **72**, 1261–1275, https://doi.org/10.1175/JAS-D-14-0216.1.

——, ——, and W. Rivera Rios, 2003: Thermal variability of the tropical tropopause region derived from GPS/MET observations. *J. Geophys. Res.*, **108**, 4024, https://doi.org/10.1029/2002JD002595.

——, D. J. Seidel, and L. L. Pan, 2007a: Observational characteristics of double tropopauses. *J. Geophys. Res.*, **112**, D07309, https://doi.org/10.1029/2006JD007904.

——, F. Wu, and P. Forster, 2007b: The extratropical tropopause inversion layer: Global observations with GPS data, and a radiative forcing mechanism. *J. Atmos. Sci.*, **64**, 4489–4496, https://doi.org/10.1175/2007JAS2412.1.

Rennie, M. P., 2010: The impact of GPS radio occultation assimilation at the Met Office. *Quart. J. Roy. Meteor. Soc.*, **136**, 116–131, https://doi.org/10.1002/qj.521.

Rieckh, T., B. Scherllin-Pirscher, F. Ladstädter, and U. Foelsche, 2014: Characteristics of tropopause parameters as observed with GPS radio occultation. *Atmos. Meas. Tech.*, **7**, 3947–3958, https://doi.org/10.5194/amt-7-3947-2014.

——, R. A. Anthes, W. Randel, S.-P. Ho, and U. Foelsche, 2017: Tropospheric dry layers in the tropical western Pacific: Comparisons of GPS radio occultation with multiple data sets. *Atmos. Meas. Tech.*, **10**, 1093–1110, https://doi.org/10.5194/amt-10-1093-2017.

——, ——, ——, ——, and ——, 2018: Evaluating tropospheric humidity from GPS radio occultation, radiosonde, and AIRS from high-resolution time series. *Atmos. Meas. Tech.*, **11**, 3091–3109, https://doi.org/10.5194/amt-11-3091-2018.

Santer, B. D., and Coauthors, 2003:Behavior of tropopause height and atmospheric temperature in models, reanalyses, and observations: Decadal changes. *J. Geophys. Res.*, **108**, 4002, https://doi.org/10.1029/2002JD002258.

Scherllin-Pirscher, B., C. Deser, S.-P. Ho, C. Chou, W. Randel, and Y. H. Kuo, 2012: The vertical and spatial structure of ENSO in the upper troposphere and lower stratosphere from GPS radio occultation measurements. *Geophys. Res. Lett.*, **39**, L20801, https://doi.org/10.1029/2012GL053071.

——, S. Syndergaard, U. Foelsche, and K. B. Lauritsen, 2015: Generation of a bending angle radio occultation climatology (BAROCLIM) and its use in radio occultation retrievals. *Atmos. Meas. Tech.*, **8**, 109–124, https://doi.org/10.5194/amt-8-109-2015.

——, W. J. Randel, and J. Kim, 2017: Tropical temperature variability and Kelvin-wave activity in the UTLS from GPS RO measurements. *Atmos. Chem. Phys.*, **17**, 793–806, https://doi.org/10.5194/acp-17-793-2017.

Schluessel, P., and W. J. Emery, 1990: Atmospheric water vapour over oceans from SSM/I measurements. *Int. J. Remote Sens.*, **11**, 753–766, https://doi.org/10.1080/01431169008955055.

Schmidt, T., S. Heise, J. Wickert, G. Beyerle, and C. Reigber, 2005: GPS radio occultation with CHAMP and SAC-C: Global monitoring of thermal tropopause parameters. *Atmos. Chem. Phys.*, **5**, 1473–1488, https://doi.org/10.5194/acp-5-1473-2005.

——, G. Beyerle, S. Heise, J. Wickert and M. Rothacher, 2006: A climatology of multiple tropopauses derived from GPS radio occultations with CHAMP and SAC-C. *Geophys. Res. Lett.*, **33**, L04808, https://doi.org/10.1029/2005GL024600.

——, J. Wickert, G. Beyerle, and S. Heise, 2008: Global tropopause height trends estimated from GPS radio occultation data. *Geophys. Res. Lett.*, **35**, L11806, https://doi.org/10.1029/2008GL034012.

——, J.-P. Cammas, H. G. J. Smit, S. Heise, J. Wickert, and A. Haser 2010: Observational characteristics of the tropopause inversion layer derived from CHAMP/GRACE radio occultations and MOZAIC aircraft data. *J. Geophys. Res.*, **115**, D24304, https://doi.org/10.1029/2010JD014284.

——, P. Alexander, and A. de la Torre, 2016: Stratospheric gravity wave momentum flux from radio occultation. *J. Geophys. Res. Atmos.*, **121**, 4443–4467, https://doi.org/10.1002/2015JD024135.

Schreiner, W. S., 2019: COSMIC and RO missions of opportunity. *JCSDA Quarterly Newsletter*, No. 62, 1–6.

——, S. V. Sokolovskiy, C. Rocken, and D. C. Hunt, 1999: Analysis and validation of GPS/MET radio occultation data in the ionosphere. *Radio Sci.*, **34**, 949–966, https://doi.org/10.1029/1999RS900034.

——, ——, D. Hunt, C. Rocken, and Y.-H. Kuo 2011: Analysis of GPS radio occultation data from the FORMOSAT-3/COSMIC and MetOp/GRAS missions at CDAAC. *Atmos. Meas. Tech.*, **4**, 2255–2272, https://doi.org/10.5194/amt-4-2255-2011.

Schröder, M., and Coauthors, 2017: GEWEX water vapor assessment (G-VAP). World Climate Research Programme Rep. 16/2017, 216 pp.

Schunk, R. W., and Coauthors, 2016: Space weather forecasting with a multimodel ensemble prediction system (MEPS). *Radio Sci.*, **51**, 1157–1165, https://doi.org/10.1002/2015RS005888.

Seidel, D. J., Q. Fu, W. J. Randel, and T. J. Reichler, 2008: Widening of the tropical belt in a changing climate. *Nat. Geosci.*, **1**, 21–24, https://doi.org/10.1038/ngeo.2007.38.

——, N. P. Gillett, J. R. Lanzante, K. P. Shine, and P. W. Thorne, 2011: Stratospheric temperature trends: Our evolving understanding. *Wiley Interdiscip. Rev.: Climate Change*, **2**, 592–616, https://doi.org/10.1002/WCC.125.

Seif, A., J.-Y. Liu, A. J. Mannucci, B. A. Carter, R. Norman, R. G. Caton, and R. T. Tsunoda, 2017: A study of daytime L-band scintillation in association with sporadic E along the magnetic dip equator. *Radio Sci.*, **70**, 360–368, https://doi.org/10.1002/2017RS006393.

Sheng, C., Y. Deng, X. Yue, and Y. Huang, 2014: Height-integrated Pedersen conductivity in both E and F regions from COSMIC observations. *J. Atmos. Sol.-Terr. Phys.*, **115–116**, 79–86, https://doi.org/10.1016/j.jastp.2013.12.013.

Shepherd, M. G., and T. Tsuda, 2008: Large-scale planetary disturbances in stratospheric temperature at high-latitudes in the southern summer hemisphere. *Atmos. Chem. Phys.*, **8**, 7557–7570, https://doi.org/10.5194/acp-8-7557-2008.

Simmons, A. J., P. Poli, D. P. Dee, P. Berrisford, H. Hersbach, S. Kobayashi, and C. Peubey, 2014: Estimating low-frequency variability and trends in atmospheric temperature using ERA-Interim. *Quart. J. Roy. Meteor. Soc.*, **140**, 329–353, https://doi.org/10.1002/qj.2317.

Sokolovskiy, S., 2003: Effect of superrefraction on inversions of radio occultation signals in the lower troposphere. *Radio Sci.*, **38**, 1058, https://doi.org/10.1029/2002RS002728.

——, Y. H. Kuo, and W. Wang, 2005: Assessing the accuracy of a linearized observation operator for assimilation of radio occultation data: Case simulations with a high-resolution weather model. *Mon. Wea. Rev.*, **133**, 2200–2212, https://doi.org/10.1175/MWR2948.1.

——, ——, C. Rocken, W. S. Schreiner, D. Hunt, and R. A. Anthes, 2006: Monitoring the atmospheric boundary layer by GPS radio occultation signals recorded in the open-loop mode. *Geophys. Res. Lett.*, **33**, L12813, https://doi.org/10.1029/2006GL025955.

——, D. Lenschow, C. Rocken, W. Schreiner, D. Hunt, Y.-H. Kuo, and R. Anthes, 2010a: Variability of the boundary layer depth over certain regions of the subtropical ocean from 3 years of COSMIC data. *14th Symp. on Integrated Observing and Assimilation Systems for the Atmosphere, Oceans, and Land Surface,* Atlanta, GA, Amer. Meteor. Soc., 534, https://ams.confex.com/ams/90annual/techprogram/paper_165488.htm.

——, C. Rocken, W. Schreinner, and D. Hunt, 2010b: On the uncertainty of radio occultation inversions in the lower troposphere. *J. Geophys. Res.*, **115**, D22111, https://doi.org/10.1029/2010JD014058.

——, W. Schreiner, Z. Zeng, D. Hunt, Y.-C. Lin, and Y.-H. Kuo, 2014: Observation, analysis, and modeling of deep radio occultation signals: Effects of tropospheric ducts and interfering signals. *Radio Sci.*, **49**, 954–970, https://doi.org/10.1002/2014RS005436.

Steiner, A. K., and G. Kirchengast, 2005: Error analysis for GNSS radio occultation data based on ensembles of profiles from end-to-end simulations. *J. Geophys. Res.*, **110**, D15307, https://doi.org/10.1029/2004JD005251.

——, ——, M. Borsche, U. Foelsche, and T. Schoengassner, 2007: A multi-year comparison of lower stratospheric temperatures from CHAMP radio occultation data with MSU/AMSU records. *J. Geophys. Res.*, **112**, D22110, https://doi.org/10.1029/2006JD008283.

——, B. C. Lackner, F. Ladstädter, B. Scherllin-Pirscher, U. Foelsche, and G. Kirchengast, 2011: GPS radio occultation for climate monitoring and change detection. *Radio Sci.*, **46**, RS0D24, https://doi.org/10.1029/2010RS004614.

——, and Coauthors, 2013: Quantification of structural uncertainty in climate data records from GPS radio occultation. *Atmos. Chem. Phys.*, **13**, 1469–1484, https://doi.org/10.5194/acp-13-1469-2013.

——, B. C. Lackner, and M. A. Ringer, 2018: Tropical convection regimes in climate models: Evaluation with satellite observations. *Atmos. Chem. Phys.*, **18**, 4657–4672, https://doi.org/10.5194/acp-18-4657-2018.

Sun, B., A. Reale, D. J. Seidel, and D. C. Hunt, 2010: Comparing radiosonde and COSMIC atmospheric profile data to quantify differences among radiosonde types and the effects of imperfect collocation on comparison statistics. *J. Geophys. Res.*, **115**, D23104, https://doi.org/10.1029/2010JD014457.

——, ——, S. Schroeder, D. J. Seidel, and B. Ballish, 2013: Toward improved corrections for radiation-induced biases in radiosonde temperature observations. *J. Geophys. Res. Atmos.*, **118**, 4231–4243, https://doi.org/10.1002/jgrd.50369.

Syndergaard, S., 2000: On the ionosphere calibration in GPS radio occultation measurements. *Radio Sci.*, **35**, 865–883, https://doi.org/10.1029/1999RS002199.

Teng, W.-H., C. Y. Huang, S.-P. Ho, Y. H. Kuo, and X. J. Zhou, 2013: Characteristics of global precipitable water in ENSO events revealed by COSMIC measurements. *J. Geophys. Res. Atmos.*, **118**, 1–15, https://doi.org/10.1002/jgrd.50371.

Thayer, J. P., J. F. Vickrey, R. A. Heelis, and J. B. Gary, 1995: Interpretation and modeling of the high-latitude electromagnetic energy flux. *J. Geophys. Res.*, **100**, 19 715–19 728, https://doi.org/10.1029/95JA01159.

Thorne, P. W., and Coauthors, 2011: A quantification of uncertainties in historical tropical tropospheric temperature trends from radiosondes. *J. Geophys. Res.*, **116**, D12116, https://doi.org/10.1029/2010JD015487.

Tian, B., C. O. Ao, D. E. Waliser, E. J. Fetzer, A. J. Mannucci, and J. Teixeira, 2012: Intraseasonal temperature variability in the upper troposphere and lower stratosphere from the GPS radio occultation measurements. *J. Geophys. Res.*, **117,** D15110, https://doi.org/10.1029/2012JD017715.

Tsuda, T., 2014: Characteristics of atmospheric gravity waves observed using the MU (middle and upper atmosphere) radar and GPS (global positioning system) radio occultation. *Proc. Japan Acad.*, **90B**, 12–27, https://doi.org/10.2183/pjab.90.12.

Tulasi Ram, S., J. Lei, S.-Y. Su, C. H. Liu, C. H. Lin, and W. S. Chen, 2010a: Dayside ionospheric response to recurrent geomagnetic activity during the extreme solar minimum of 2008. *Geophys. Res. Lett.*, **37**, L02101, https://doi.org/10.1029/2009GL041038.

——, C. H. Liu, and S.-Y. Su, 2010b: Periodic solar wind forcing due to recurrent coronal holes during 1996–2009 and its impact on Earth's geomagnetic and ionospheric properties during the extreme solar minimum. *J. Geophys. Res.*, **115**, A12340, https://doi.org/10.1029/2010JA015800.

——, S.-Y. Su, L.-C. Tsai, and C. H. Liu, 2016: A self-contained GIM-aided Abel retrieval method to improve GNSS-radio occultation retrieved electron density profiles. *GPS Solutions*, **20**, 825–836, https://doi.org/10.1007/s10291-015-0491-z.

Vergados, P., A. J. Mannucci, and H. Su, 2013: A validation study for GPS radio occultation data with moist thermodynamic structure of tropical cyclones. *J. Geophys. Res. Atmos.*, **118**, 9401–9413, https://doi.org/10.1002/jgrd.50698.

——, Z. J. Luo, K. Emanuel, and A. J. Mannucci, 2014: Observational tests of hurricane intensity estimations using GPS radio occultations. *J. Geophys. Res. Atmos.*, **119**, 1936–1948, https://doi.org/10.1002/2013JD020934.

Virts, K. S., and J. M. Wallace, 2014: Observations of temperature, wind, cirrus, and trace gases in the tropical tropopause transition layer during the MJO. *J. Atmos. Sci.*, **71**, 1143–1157, https://doi.org/10.1175/JAS-D-13-0178.1.

von Engeln, A., S. Healy, C. Marquardt, Y. Andres, and F. Sancho, 2009: Validation of operational GRAS radio occultation data. *Geophys. Res. Lett.*, **36**, L17809, https://doi.org/10.1029/2009GL039968.

Wang, L., and M. J. Alexander, 2010: Global estimates of gravity wave parameters from GPS radio occultation temperature data. *J. Geophys. Res.*, **115**, D21122, https://doi.org/10.1029/2010JD013860.

Ware, R., and Coauthors, 1996: GPS sounding of the atmosphere from low Earth orbit: Preliminary results. *Bull. Amer. Meteor. Soc.*, **77**, 19–40, https://doi.org/10.1175/1520-0477(1996)077<0019:GSOTAF>2.0.CO;2.

Wee, T.-K., and Y.-H. Kuo, 2014: A perspective on the fundamental quality of GPS radio occultation data. *Atmos. Meas. Tech. Discuss.*, **7**, 9481–9508, https://doi.org/10.5194/amtd-7-9481-2014.

Wentz, F. J., 2015: A 17-year climate record of environmental parameters derived from the Tropical Rainfall Measuring Mission (TRMM) Microwave Imager. *J. Climate*, **28**, 6882–6902, https://doi.org/10.1175/JCLI-D-15-0155.1.

——, and R. W. Spencer, 1998: SSM/I rain retrievals within a unified all-weather ocean algorithm. *J. Atmos. Sci.*, **55**, 1613–1627, https://doi.org/10.1175/1520-0469(1998)055<1613:SIRRWA>2.0.CO;2.

Wick, G. A., Y.-H. Kuo, F. M. Ralph, T.-K. Wee, P. J. Neiman, and Z. Ma, 2008: Intercomparison of integrated water vapor retrievals from SSM/I and COSMIC. *Geophys. Res. Lett.*, **28**, 3263–3266, https://doi.org/10.1029/2008GL035126.

Wilhelmsen, H., F. Ladstädter, B. Scherllin-Pirscher, and A. K. Steiner, 2018: Atmospheric QBO and ENSO indices with high vertical resolution from GNSS radio occultation temperature measurements. *Atmos. Meas. Tech.*, **11**, 1333–1346, https://doi.org/10.5194/amt-11-1333-2018.

Wu, D. L., 2018: New global electron density observations from GPS-RO in the D- and E-region ionosphere. *J. Atmos. Sol.-Terr. Phys.*, **171**, 36–59, https://doi.org/10.1016/j.jastp.2017.07.013.

Xie, F., S. Syndergaard, E. R. Kursinski, and B. Herman, 2006: An approach for retrieving marine boundary layer refractivity from GPS occultation data in the presence of superrefraction. *J. Atmos. Oceanic Technol.*, **23**, 1629–1644, https://doi.org/10.1175/JTECH1996.1.

——, D. L. Wu, C. O. Ao, and A. J. Mannucci, 2010a: Atmospheric diurnal variations observed with GPS radio occultation soundings. *Atmos. Chem. Phys.*, **10**, 6889–6899, https://doi.org/10.5194/acp-10-6889-2010.

——, ——, ——, ——, and S. Syndergaard, 2010b: Super-refraction effects on GPS radio occultation refractivity in marine boundary layers. *Geophys. Res. Lett.*, **37**, L11805, https://doi.org/10.1029/2010GL043299.

——, ——, ——, ——, and E. R. Kursinski, 2012: Advances and limitations of atmospheric boundary layer observations with GPS occultation over southeast Pacific Ocean. *Atmos. Chem. Phys.*, **12**, 903–918, https://doi.org/10.5194/acp-12-903-2012.

Yang, S.-C., S.-H. Chen, S.-Y. Chen, C.-Y. Huang, and C.-S. Chen, 2014: Evaluating the impact of the COSMIC RO bending angle data on predicting the heavy precipitation episode on 16 June 2008 during SoWMEX-IOP8. *Mon. Wea. Rev.*, **142**, 4139–4163, https://doi.org/10.1175/MWR-D-13-00275.1.

Yue, X., W. S. Schreiner, J. Lei, C. Rocken, D. C. Hunt, Y.-H. Kuo, and W. Wan, 2010a: Global ionospheric response observed by COSMIC satellites during the January 2009 stratospheric sudden warming event. *J. Geophys. Res.*, **115**, A00G09, https://doi.org/10.1029/2010JA015466.

——, ——, ——, S. V. Sokolovskiy, C. Rocken, D. C. Hunt, and Y.-H. Kuo, 2010b: Error analysis of Abel retrieved electron density profiles from radio occultation measurements. *Ann. Geophys.*, **28**, 217–222, https://doi.org/10.5194/angeo-28-217-2010.

Yue, X., W. S. Schreiner, Y.-C. Lin, C. Rocken, Y.-H. Kuo, and B. Zhao, 2011: Data assimilation retrieval of electron density profiles from radio occultation measurements. *J. Geophys. Res.*, **116**, A03317, https://doi.org/10.1029/2010JA015980.

——, and Coauthors, 2012: Global 3-D ionospheric electron density reanalysis based on multisource data assimilation. *J. Geophys. Res.*, **117**, A09325, https://doi.org/10.1029/2012JA017968.

——, W. S. Schreiner, and Y.-H. Kuo, 2013: Evaluating the effect of the global ionospheric map on aiding retrieval of radio occultation electron density profiles. *GPS Solutions*, **17**, 327–335, https://doi.org/10.1007/s10291-012-0281-9.

——, ——, N. Pedatella, R. A. Anthes, A. J. Mannucci, P. R. Straus, and J.-Y. Liu, 2014: Space weather observations by GNSS radio occultation: From FORMOSAT-3/COSMIC to FORMOSAT-7/COSMIC-2. *Space Wea.*, **12**, 616–621, https://doi.org/10.1002/2014SW001133.

——, ——, ——, and Y.-H. Kuo, 2016: Characterizing GPS radio occultation loss of lock due to ionospheric weather. *Space Wea.*, **14**, 285–299, https://doi.org/10.1002/2015SW001340.

Yunck, T. P., C.-H. Liu, and R. Ware, 2000:A history of GPS sounding. *Terr. Atmos. Ocean. Sci.*, **11**, 1–20, https://doi.org/10.3319/TAO.2000.11.1.1(COSMIC).

Zeng, Z., and S. Sokolovskiy, 2010: Effect of sporadic E clouds on GPS radio occultation signals. *Geophys. Res. Lett.*, **37**, L18817, https://doi.org/10.1029/2010GL044561.

——, W. Randel, S. Sokolovskiy, C. Deser, Y.-H. Kuo, M. Hagan, J. Du, and W. Ward, 2008: Detection of migrating diurnal tide in the tropical upper troposphere and lower stratosphere using the Challenging Minisatellite Payload radio occultation data. *J. Geophys. Res.*, **113**, D03102, https://doi.org/10.1029/2007JD008725.

——, S.-P. Ho, S. Sokolovskiy, and Y.-H. Kuo, 2012: Structural evolution of the Madden-Julian oscillation from COSMIC radio occultation data. *J. Geophys. Res.*, **117**, D22108, https://doi.org/10.1029/2012JD017685.

——, S. Sokolovskiy, W. S. Schreiner, and D. Hunt, 2019: Representation of vertical atmospheric structures by radio occultation observations in the upper troposphere and lower stratosphere: Comparison to high-resolution radiosonde profiles. *J. Atmos. Oceanic Technol.*, **36,** 655–670 https://doi.org/10.1175/JTECH-D-18-0105.1.

Zou, X., L. Lin, and F. Weng, 2014: Absolute calibration of ATMS upper level temperature sounding channels using GPS RO observations. *IEEE Trans. Geosci. Remote Sens.*, **52**, 1397–1406, https://doi.org/10.1109/TGRS.2013.2250981.